SIMULATION OF NUCLEAR RESONANCE FLUORESCENCE FOR THE QUANTIFICATION OF PLUTONIUM-239 IN NUCLEAR FUEL

A Thesis

by

JEREMY JENS GERHART

Submitted to the Office of Graduate and Professional Studies of Texas A&M University
in partial fulfillment of the requirements for the degree of

MASTER OF SCIENCE

Chair of Committee, William Charlton
Committee Members, David Boyle
Michael Schuller
Head of Department, Yassin Hassan

December 2015

Major Subject: Nuclear Engineering

ABSTRACT

There is a need for a technique that is able to quickly and accurately quantify the amount of ^{239}Pu in spent nuclear fuel. With the recent developments of mono-energetic gamma-ray systems, it may be possible to use Nuclear Resonance Fluorescence for this task. Previous gamma-ray sources for the technique were Bremsstrahlung sources. There was a distinct disadvantage with this technique due to the broad energy spectrum that Bremsstrahlung sources create. However, at Lawrence Livermore National Laboratory a new source has been developed which uses Compton scattering of photons off of electrons to create extremely thin energy bandwidth gamma-rays.

In this research a Monte Carlo code developed by Lawrence Livermore National Laboratory, known as COG, was used to investigate detector designs for use with mono-energetic gamma-ray sources to quantify plutonium in spent nuclear fuel assemblies. It is shown that the technique is viable for the quantification of plutonium in fresh and spent mixed oxide fuel. However, these calculations suggest that Nuclear Resonance Fluorescence is not sufficiently sensitive for low plutonium-239 concentrations, <1% atom percent, which is the concentration present in spent pressurized water reactor fuel. Investigation into the lack of sensitivity was inconclusive. A more in-depth analysis of COG's capabilities in this area should be conducted.

DEDICATION

This thesis is dedicated to my family: Dennis, Kathy, and Josh. Without their love and support I would not be where I am today.

ACKNOWLEDGEMENTS

I would like to thank my committee chair and advisor, Dr. William Charlton. He has pushed me to become the best engineer that I can be.

I would also like to thank Dr. David Boyle and Dr. Michael Schuller for their guidance and assistance throughout this research.

Thanks go to my collaborators at Lawrence Livermore National Laboratory, Dr. Christopher P. J. Barty and Dr. James Hall, they were invaluable during this research.

Finally, I would like to thank my friends at Texas A&M and my family for the support that they gave me.

TABLE OF CONTENTS

Page

LIST OF FIGURES

Page

LIST OF TABLES

Page

1. INTRODUCTION

1.1 Statement of the Problem

There is a need to develop techniques that can accurately quantify the amount of plutonium in spent nuclear fuel. The large amount of background radiation emitted by decay products and transuranics in the fuel assemblies makes this a difficult task. New interrogation sources are being developed to make this task easier. One of these sources is called a Mono-Energetic Gamma-Ray source, or MEGa-Ray source.[1] With a high enough energy photon source it is possible to interrogate the nuclei instead of valence electrons. In this research a Monte Carlo code developed by Lawrence Livermore National Laboratory (LLNL), known as COG, was used to investigate the use of MEGa-Ray sources to quantify plutonium in spent nuclear fuel assemblies. The goal of the research was to determine the accuracy with which ^{239}Pu can be quantified in Pressurized Water Reactor (PWR) spent nuclear fuel (SNF) assemblies using a MEGa-Ray source.

1.2 Explanation of Safeguards

The term "safeguards" is defined in INFCIRC-153 as a broad range of techniques/systems designed to detect the diversion of nuclear material from peaceful purposes and the misuse of technologies for undeclared production of nuclear material.[2] The international safeguards system is maintained by the International Atomic Energy Agency (IAEA). The IAEA's safeguards system consists of a variety of technical mechanisms, including material control and accountancy, containment, and

surveillance.[3] A diversion of nuclear material is defined as the undeclared removal of material or the use of declared nuclear facilities for undeclared purposes.[4] The term "significant quantity" (SQ) refers to amounts of various nuclear materials for which the IAEA cannot exclude that a state would be able to manufacture a nuclear weapon. The IAEA declared SQs are shown in **Table 1-1**.

Table 1-1 IAEA declared significant quantities of direct and indirect use materials

Reprinted from [4]

Material	Significant Quantity
Direct Use Nuclear Material	
Pu	8 kg Pu
^{233}U	8 kg ^{233}U
HEU ($^{235}U \geq 20\%$)	25 kg ^{235}U
Indirect Use Nuclear Material	
U ($^{235}U < 20\%$)	75 kg ^{235}U (or 10 t natural U or 20 t depleted U)
Th	20 t Th

Depending on the source of the nuclide there is a varying amount of time which may be required to convert the material into the required form for use in a nuclear weapon. Ranges for various source materials are shown in **Table 1-2**. The associated timelines for the materials were obtained from the IAEA.[4]

Table 1-2 Estimated conversion times and timeliness goals for direct and indirect materials Reprinted from [4]

Beginning Material Form	Conversion Time	Timeliness Goals
Pu, HEU, or ^{235}U Metal	Order of Days (7-10)	1 month
PuO_2, $Pu(NO_3)_4$, or other pure Pu compounds; HEU or ^{233}U oxide or other pure U compounds; MOX or other non-irradiated pure mixtures containing Pu, U (^{233}U + $^{235}U \geq 20\%$); Pu, HEU, and/or ^{233}U in scrap or other miscellaneous impure compound	Order of weeks (1-3)	1 month
Pu, HEU, or ^{233}U in irradiated fuel	Order of months (1-3)	3 months
U containing <20% ^{235}U and ^{233}U; Th	Order of months (3-12)	1 year

Identifying the theft or diversion of significant quantities of nuclear materials requires safeguards techniques that can provide quantification of nuclear materials within specified accuracy limits. The level of accuracy is dependent on the nuclide of interest and the material composition. A significant quantity of plutonium is identified by the IAEA as 8 kilograms, provided the content of ^{238}Pu is less than 80%. This value includes unavoidable losses during the separation of plutonium and fabrication of the physics package for the weapon.[4] The IAEA has set timeliness detection goals for various materials. For plutonium in SNF, the timeliness goal is 3 months. By combining the information from **Table 1-1** and the timeliness goal, the accuracy limit for ^{239}Pu can be identified.

Safeguards systems must be able to quantify plutonium to within a 3-sigma uncertainty of 8 kg in less than 3 months, if in irradiated fuel, in order to meet the goals of the IAEA.[4]

1.3 Why Quantification of Plutonium is Important

Accurate quantification of plutonium in SNF is an extremely important aspect of safeguards due to the need to detect diversion of significant quantities of nuclear material. The primary way to obtain plutonium is via chemical separation from SNF that has been discharged from nuclear reactors. The quantity and composition of the spent fuel assemblies can vary drastically depending on the type of reactor in which the assembly was irradiated. Reactors of concern for this research are commercial Light Water Reactors (LWRs), specifically PWRs. Plutonium production occurs via a variety of paths in a nuclear reactor. These reaction pathways are shown in ***Figure 1.1***. It is important to note that the bold outlines on ^{234}U, ^{235}U, and ^{238}U represent the nuclides that are present in the fuel assembly prior to irradiation.[5] The colors represent half-life ranges on the Chart of the Nuclides.

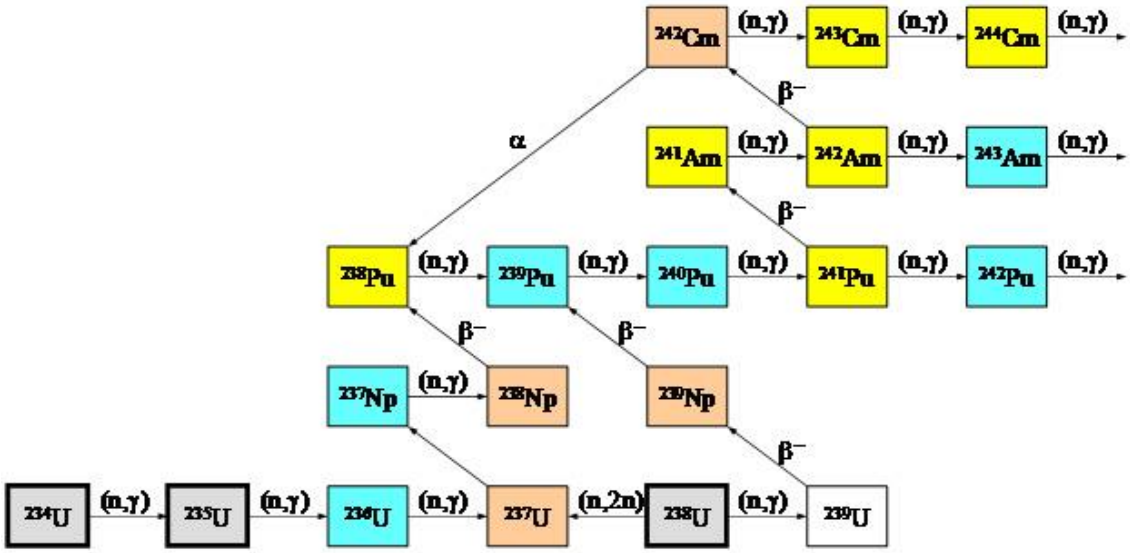

Figure 1.1 *Plutonium production mechanisms in a nuclear reactor*

The fuel assemblies in PWRs typically consist of a 17 x 17 array of fuel pins; however, other array configurations have been used. A reactor core has a large number of assemblies, usually between 120-200 assemblies, in it during operation. The exact number depends on the design of the reactor.[6] The reactor is typically refueled every 1.5 years. During refueling the assemblies are typically shuffled in order to maintain a smooth power profile in the reactor, roughly 1/3 of the assemblies are discharged and unirradiated assemblies are inserted. This results in a discharge of roughly 300 kg, or almost 38 SQs, of plutonium every refueling cycle.[7] **Table 1-3** lists percent composition for each isotope in typical spent nuclear fuel that has been discharged from a PWR for various initial enrichments and the typical burn-up for the enrichment. This data was obtained from the IAEA's VISTA project.[8]

Table 1-3 Typical isotopic plutonium percentages for spent fuel discharged from PWRs Reprinted from [8]

Initial Enrichment (% ^{235}U)	Burn Up (GWd/t)	Percent Composition of Plutonium (%)				
		^{238}Pu	^{239}Pu	^{240}Pu	^{241}Pu	^{242}Pu
1.35	5	0.09	83.04	14.02	2.67	0.17
1.7	10	0.00	73.71	19.62	5.79	0.67
2.05	15	0.00	67.43	22.55	8.29	1.35
2.4	20	0.01	62.87	24.21	10.22	2.11
2.75	25	0.01	59.39	25.16	11.69	2.92
3.1	30	0.01	56.62	25.69	12.80	3.74
3.4	35	0.02	54.17	25.97	13.71	4.64
3.7	40	0.02	52.13	26.03	14.37	5.53
4	45	0.20	41.40	21.33	12.19	5.26
4.25	50	0.03	48.76	25.77	15.18	7.33
4.5	55	0.04	47.35	25.51	15.38	8.21
4.8	60	0.04	46.20	25.22	15.45	8.95
5.05	65	0.05	45.08	24.88	15.46	9.74
5.35	70	0.06	44.15	24.54	15.40	10.37

Typical reactor enrichments are between 2-5% depending on the burn-up goal.[9] Using the data from **Table 1-3** and the amount of total plutonium discharged from a nuclear reactor per refueling cycle, 300 kg Pu, the amount of ^{239}Pu discharged per refueling cycle is typically between ~120-200 kg.

Due to the large amount of plutonium discharged by a single reactor during a refueling cycle, it is extremely important to create safeguards systems capable of quantifying the plutonium content of spent fuel assemblies. Without an accurate way of determining how many SQs of plutonium are being discharged from the reactors, the potential for diversion

is high. Just as important is the time required for quantifying the plutonium. Timeliness is important because of the large number of spent fuel assemblies being discharged from a reactor, roughly 40-65 per 1.5 year refueling cycle, and the significant amount of plutonium that is discharged every refueling cycle, around 300 kg per refueling.[6,7] With that many assemblies being discharge per refueling, the total number of assemblies stored in spent fuel pools at reactors can be extremely large. As a result, it is important that the amount of time to assay each assembly be short. In addition, the time between assays must be short due to the amount of time required to convert the plutonium in spent nuclear fuel, 1-3 months.[4]

1.4 Current Techniques

Currently there are no methods acceptably accurate or timely enough to directly measure plutonium in spent nuclear fuel. Plutonium passively emits characteristic γ-rays in the 200-600 keV range and spontaneous fission neutrons that, in principle, could be used to quantitatively measure Pu content in spent fuel. However, the low percentage of Pu in spent fuel (~1% by mass for PWR fuel and 6% by mass for MOX Fuel) means these signatures are overwhelmed by the large amount of background radiation emitted by the decay of fission products, transuranic products, and activated structural components. This background radiation consists of both gamma-rays and neutrons and has a broad energy range. In addition, the high density of the nuclear material means that there is significant attenuation of γ-ray signals in the 200-600 keV range. Therefore, various indirect measurement techniques are employed instead. For example, a measurement of gross γ and neutron emission from an assembly can be correlated to burnup and cooling time.

These values are then used to estimate the plutonium content of the assembly using computationally simulated data. In order to obtain the spent fuel isotopics, a burn-up code must be used, such as CINDER[10] or ORIGEN[11]. The initial fuel assembly is modeled in the code and then irradiated to the appropriate burnup and cooling time which were obtained through the measurements of the fuel assembly. This calculation outputs the spent fuel isotopics (including Pu content). The resulting values from the measurements and simulations are compared to the operator declared values for the assemblies. Various other techniques have been studied for safeguarding spent nuclear fuel.[12] The various techniques for measuring Pu content in SNF assemblies are discussed in more detail below.

1.4.1 Total Gamma-Ray Activity

One of the techniques used to characterize spent nuclear fuel is to use ion chambers, scintillators, or thermoluminescent dosimeters to measure total gamma-ray dose rate from the assemblies. In these measurements, the fuel assemblies are raised out of the storage racks in the spent fuel pool, while still being submerged in the water, and the measurement is taken. By removing the assembly from the storage rack, the radiation from adjacent assemblies in the storage rack does not interfere with the results. The total gamma-ray activity of the assembly is then used to estimate the burn-up and cooling time of the reactor. It has been determined that burn-up and cooling time, which are linked to plutonium content, can be estimated to within 10% using this technique.[12] The currently deployed systems that utilize this technique are known as FORK[13] and SMOPY[14]. The FORK detector uses ion chambers, positioned on opposite sides of the assembly to

determine the total gamma-ray emissions. These ion chambers are housed in polyethylene in the shape of a "U". SMOPY has a cylindrical shape and uses a micro room temperature gamma spectrometric probe that is shielded by tungsten. Both the FORK and SMOPY systems also employ neutron measurements through the use of fission chambers.

1.4.2 High-Resolution Gamma-Ray Spectroscopy

In this technique, a germanium detector is used to obtain a high-resolution gamma-ray spectrum. The spectrum is then analyzed for specific emission peaks from the decay of fission products, such as ^{134}Cs, ^{137}Cs, and ^{154}Eu. The area of the emission peaks is then converted to activity, and by using a combination of the ratios between the fission products, the burn-up and cooling time can be estimated. This technique poses a few problems: the system is typically difficult to move due to the cooling requirements of germanium and the large amount of shielding that must be present to prevent background radiation from impacting the measurements. Additionally, a large stand-off distance must be used between the detector and the assembly to limit the impact of the background radiation being emitted from the assembly. Overall, this results in a large footprint for the system, which is not desirable for the reactor operators. However, the technique does provide excellent precision and accuracy with 4-8% agreement to declared burn-ups.[12]

1.4.3 High-Energy Gamma-Ray Activity

It is possible to use a more specific gamma-ray measurement by making use of a ^{235}U fission chamber surrounded by polyethylene, which is then surrounded by beryllium. The detector system makes use of the photonuclear cross-section of beryllium. When a

gamma-ray with energy greater than 1.665 MeV interacts with the beryllium, a neutron is produced. This neutron is then thermalized in the polyethylene, which will then cause a fission in the ^{235}U. There is only one significant fission product that emits a gamma with a high enough energy to overcome this threshold - ^{144}Ce-Pr. The activity of the ^{144}Ce-Pr is then correlated to burn-up and cooling time. The downfall of this technique is that it is possible for neutrons emitted from the spent fuel assembly to register counts in the fission chamber, as well as neutrons from (n, 2n) reactions that occur in the beryllium.[12]

1.4.4 Neutron Measurements of Irradiated Fuel

Neutron measurements are relatively quick and easy to make and can provide estimates of assembly burn-up. Any type of neutron detector can be used to make the measurements; however, fission chambers are preferred due to their lack of gamma-ray sensitivity. One of the major downsides to this technique is neutrons are easily attenuated by water, which means the detector must be placed as close to the assembly as possible. In these techniques, total neutrons are measured and used to determine an overall activity for the assembly. The main contributor to the neutron emission from the assembly is curium. The amount of curium is related to the burnup and cooling time of the fuel; as such, the number of measured neutrons is correlated to the amount of curium, which is then correlated to burnup and cooling time.[12]

1.5 Why Use Nuclear Resonance Fluorescence?

Nuclear Resonance Fluorescence (NRF) was discovered by Rudolf Mössbauer in 1958.[15] In more recent years, it has been proposed as a technique for safeguards.[16–

18] NRF has been investigated for use in identifying nuclear weapons/material being transported in cargo containers/vehicles[16] and has also been proposed as a technique to quantify plutonium in spent nuclear fuel.[17,18] Both of these investigations showed promise for the technique to be used as a safeguards system. NRF allows the nucleus of a specific nuclide to be interrogated, which provides a degree of measurement specificity that current techniques do not possess. The system can be set up to interrogate any nuclide, provided the energy of absorption is known and a system exists to provide a source of photons at that precise absorption energy.

1.6 How Nuclear Resonance Fluorescence Works

NRF reactions are similar to more traditional atomic fluorescence in which a photon of a specific energy, incident on a sample, is absorbed by a valence electron and a photon of lesser energy is emitted at a later time. The primary difference between traditional fluorescence and NRF is that instead of exciting the molecule or atom by causing a vibration of the molecular bonds or valence electrons, the nucleons in an individual nucleus are excited. The nucleus then emits one or more photons at a slightly lower energy, and the difference between the initial and emitted energies takes the form of recoil energy for the nucleus. The emitted NRF photon(s) have essentially an isotropic angular distribution. [16]

Each nuclide has a set of specific photon energies for which an NRF interaction can occur. These incident energies are dependent on the possible excited nuclear states. In addition, the number of nucleons is important because the energies of the allowed excited nuclear states are dependent upon this number. Both the resonance energies and the cross-

sections for each energy can be determined experimentally.[16] As such, it is possible to isolate an energy for NRF interactions for a specific nuclide (e.g., ^{239}Pu) that may be above potential background sources and separated from other nuclei's NRF energies.

1.7 Mono-Energetic Gamma-Ray Sources

Mono-Energetic Gamma-Ray (MEGa-Ray) sources have been proposed and designed since 1969[1], and have utilized various techniques and reactions to produce the photons.[19,20] Recent developments of Mono-Energetic Gamma-Ray (MEGa-Ray) sources at Lawrence Livermore National Laboratory (LLNL) have resulted in a prototype source.[21,22] These sources are able to produce gamma-rays that have tunable energies. The primary advantage of these systems is the ability to produce high energy gamma-rays with sufficient energy to excite the nucleus of an atom. Previous laser systems were only able to excite the valence electrons due to their energy and intensity limitations. MEGa-Ray sources are being used to excite specific NRF reactions in various nuclides of interest. Specifically, this source type has been shown to be able to detect ^{7}Li that was shielded by lead.[23] New systems are being developed to produce higher energy gamma-rays to interrogate ^{239}Pu and uranium isotopes. This system is called the Very Energetic Light for the Observation and Characterization of Isotopic Resonances and the Assay and Precision Tomography of Objects with Radiation (VELOCIRAPTOR) and is expected to provide beams of gamma-rays with energies between 0.5-2.5 MeV.[24,25]

LLNL's MEGa-Ray sources create gamma-rays through the use of Compton scattering. This is accomplished through the use of short laser pulses incident on a relativistic electron beam. The photons from the laser collide with the electrons via

Compton scattering and produce photons that have varying energies based on the angle of the Compton scattering. The overall energy of the resulting Compton scattered photons can be adjusted by adjusting the speed of the relativistic electrons. The photons are then collimated to reduce spreading of energies, which results in the creation of a near mono-energetic beam of photons with a small bandwidth.[20]

1.8 Previous Research on Applying NRF to Safeguards

Research on NRF applications to safeguards has been conducted all over the world. In this research there is a mixture of both simulation and experimental results using a variety of techniques.[17,26–30] In addition, research investigations have been conducted to compile the capabilities of current measurements systems and assess the practical application of NRF techniques to known safeguards applications. Due to the proposed capabilities of NRF to detect nuclear material, a study was conducted to apply NRF to other illicit materials.[31] This non-nuclear application demonstrates the capabilities and strengths of using NRF to identify specific materials.

1.8.1 Lawrence Berkeley National Laboratory/University of California-Berkeley

A series of Monte Carlo N-Particle eXtended (MCNPX)[32] simulations were used to assess the viability of using NRF to measure plutonium mass in spent nuclear fuel. Included in this research was an analysis of MCNPX's capability to properly model the various reactions that occur at the high-energies where NRF interactions occur. Two primary techniques were investigated: the backscattering method and the transmission method. In each technique a bremsstrahlung source was used to induce the NRF events

in the fuel. Both techniques had problems, so it was deemed that with the state of technology it would not be possible to quantify plutonium content in spent nuclear fuel.[27]

The backscattering method had three main issues: there was a low signal-to-background ratio for the small Pu concentrations in the spent nuclear fuel, there was a high background due to the radioactive decay occurring in the fuel, and there was a strong dependence on where the NRF event occurred within the fuel assembly to whether the emission photon could be detected or not. Due to bremsstrahlung sources providing broad gamma-ray spectrums instead of discrete energies, and the detection limitations of current detector systems, these issues cannot be currently resolved.[27]

Transmission methods however have advantages over the backscattering methods because the transmission technique includes an additional sample of the material around which the detectors are positioned. This approach allows shielding to be placed between the detectors and the spent fuel assembly and also means that the NRF emission photons must only escape the small sample instead of the fuel assembly in order to be detected. However, due to the use of bremsstrahlung sources the technique was still deemed unviable because the measurements would take 10-100s of hours to finish one assembly. It was posited that by using a MEGa-Ray source it could be possible to reduce the amount of time by a factor of 100 or more.[26]

Based on the information gleaned from the simulations, a transmission measurement was conducted on a mixture of ^{238}U and Pb. In the experiment, the target material had a ^{238}U percent ranging from 0-8.5% of the total atoms. Using the detector responses, the

amount of ^{238}U content in the samples was estimated in the form of areal densities and compared to the actual areal densities obtained from direct measurements of the samples. The results showed the technique was capable of accurately measuring the ^{238}U content at 1% levels.[33]

1.8.2 International Research

A collaboration between the Japan Atomic Energy Agency (JAEA), Kyoto University, the National Institute of Advanced Industrial Science and Technology, and the High Intensity γ-ray Source (HIγS) facility demonstrated the ability to use $LaBr_3$(Ce) detectors in the transmission measurement technique. The research compared the measured results from the $LaBr_3$(Ce) detectors to the results from HPGe detectors. In this experiment, the nuclide of interest was ^{11}B, in the form of B_4C blocks. It was possible to identify a clear and statistically significant NRF emission peak in the $LaBr_3$(Ce) detectors.[29]

The JAEA and LLNL conducted an investigation into the statistical uncertainties in an NRF measurement in spent nuclear fuel. In the study, an intense mono-energetic photon beam was incident on a spent nuclear fuel assembly. The background emitted from the assembly was calculated using ORIGEN2.2-UPJ. Coherent scattering contributions from Rayleigh, Thomson, and Delbrück events were accounted for in the study. It was concluded that it is possible to assay 1% actinide content in spent nuclear fuel with a 2.2-3.2% uncertainty during a 4000 second counting period.[28]

1.8.3 Lawrence Livermore National Laboratory

LLNL has been one of the leading developers of MEGa-Ray sources. This has provided them with prototype systems that were used for various NRF applications. The major focus has been on applying NRF to safeguards scenarios. To accomplish this, an investigation using a Bremsstrahlung source to excite ^{235}U and ^{239}Pu was conducted.[16] More recently, a study of the efficacy of using an NRF system coupled with a Compton scattering photon source was completed. In this study, various detector geometries were investigated as well as a variety of possible scenarios where the measurements would be taken.[30] As a result of all of the research conducted at LLNL, a patent has been granted for a detection system known as the Dual Isotope Notch Observer (DINO).[34] This detector uses two witness pieces with backscatter detectors surrounding each witness piece. In the measurements, the two witness pieces must be the same atomic material, however each is a different isotope. For NRF measurements of ^{239}Pu, a piece of ^{239}Pu and a piece of ^{240}Pu were used as the witnesses. This allows one witness piece to NRF and scatter, while the other only has scattering interactions.

1.9 Overview of Research

The primary goal of this research was to determine the accuracy with which ^{239}Pu can be quantified in PWR SNF using a MEGa-Ray system. This work was accomplished using the Monte Carlo particle transport code COG, also developed at LLNL, and the code's NRF capability. The code was used to model the interactions between the MEGa-Ray beam and a spent nuclear fuel assembly and assess detection capability to accurately quantify the ^{239}Pu mass in the fuel assemblies. Verification tests of the physics in COG

as well as geometric capabilities of COG were performed. Following this, simulations were performed with the MEGa-RAY beam interrogating spent fuel. The results from those simulations were analyzed and conclusions on the accountancy capability of NRF using MEGa-Ray were drawn.

2. CREATION OF THE NRF DETECTION SYSTEM COMPUTATIONAL MODEL

2.1 Overview

Creation of the COG input file was carried out over multiple iterations to ensure that components of the system were being added correctly and were not adversely affecting the physics of the simulations. Extremely basic geometries were created and complexities were slowly added until the full system had been created. The initial geometry consisted of a MEGa-Ray source incident on a witness piece, which was surrounded by detectors. Various detector tally types were tried until a suitable one was found.

The sample that was to be interrogated and a collimator following the sample were added. The purpose of the collimator was to prevent undesirable gamma-rays, from Compton and photoelectric reactions in the sample, from reaching the detectors. The sample started as a simple block, then proceeded to a single fuel pin. This individual pin was then replicated to create the 17 x 17 array of pins that constituted the spent fuel assembly. The spacing parameters and dimensions of the collimator were adjusted to prevent the detectors from counting anything except emissions from interactions in the witness piece.

2.2 Geometric Configuration

In any NRF measurement, there are three portions of the system that must exist: the gamma-ray source, the sample, and a gamma-ray detection system. In this research, a mono-energetic, coherent, and spatially homogeneous beam of photons was used as the interrogating source. In actuality, the MEGa-Ray source has a small change in gamma

energy when measured off the center point of the beam, but this was ignored in the simulations. This beam was then collimated to produce a smaller diameter beam of the desired energy.[20] The interrogated samples were PWR SNF assemblies. The composition of these spent fuel assemblies was obtained from Next Generation Safeguards Initiative's Spent Fuel project (NGSI-SF).[35] The detection method that was used involved setting up an array of gamma detectors surrounding a witness piece. The witness piece is a pure sample of the nuclide of interest for the measurements. Pure ^{239}Pu was used for this research. Impure materials can be used, but the efficiency of the system will be decreased. A pure sample of ^{239}Pu was used to reduce the computational time required to obtain the results. The purpose of the witness piece is to increase the signal to noise ratio in the detectors. Due to the NRF resonance, NRF photons are more likely to interact in the witness piece by NRF absorption and be re-emitted isotropically, meaning they can enter the detectors. Other photons will not reach the detectors at the NRF energies because of the mechanics of photon interactions.

If the witness piece were not used, the detectors would have to be positioned such that they directly measured the photons emitted by NRF events in the spent fuel assembly, which would present a variety of problems. Spent fuel assemblies emit a very large amount of gamma-rays due to decay products and transuranics created during irradiation. These gamma-rays create a high level of background/noise, which increases the dead time of the detection system. Dead time is the minimum amount of time which two events in the detector must be separated in order for the events to be counted separately. If sufficient time does not separate the events, they will not be counted properly. The number of

improperly counted events can be extremely high when the detector is exposed to a high flux.[36] It is therefore important to take whatever measures can be made to reduce the background/noise incident on the detector. In addition, the spent fuel pins would scatter the photons emitted from the NRF reactions, which would complicate the isolation of these gamma-rays from the decay gamma-rays.

For an NRF interrogation, two measurements are taken. One measurement is taken without a sample in place. A measurement is also taken with a sample in place. The difference in signal from the detectors for the "no sample" and "sample present" cases is used to determine the concentration of the nuclide of interest in the sample.

In the image of the initial geometry seen in ***Figure 2.1***, the red block corresponds to the MEGa-Ray source with its emitted gamma-ray beam represented by the line leaving the block. The photons pass through the fuel assembly (dark grey) and then through the collimator (blue). The photons then reach the witness piece (yellow) and the resulting emissions/interactions are measured by the detectors (light grey). In the diagram, the distance between components and also the relative size of the components are not to scale. The spacing/sizes were chosen to ensure that all aspects of the geometry were easily distinguishable. Details on the spacing and sizes can be found in the example input provided in the **Appendix A**.

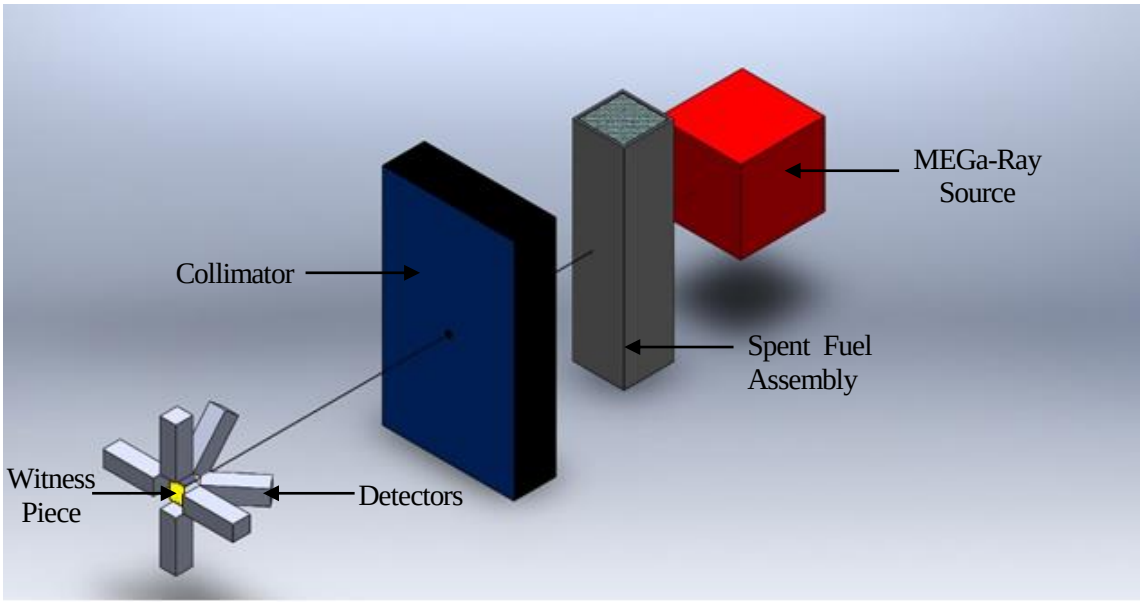

Figure 2.1 *Diagram of initial NRF detection system geometry*

Three possible detector positions around the witness piece were investigated: detectors completely surrounding the witness piece, detectors covering the forward scattering region, and detectors covering the back-scattering region. Based on the literature review of previous NRF applications for quantifying ^{239}Pu, a back-scattering technique was selected. The back-scattering technique is advantageous due to reactions that occur in the witness piece. By placing the detectors up-stream of the source and out of the path of the incoming beam, between the witness piece and the collimator shield, the un-collided source photons will not be counted. Any contribution due to single Rayleigh scattering can be eliminated. The energy of Compton scatter secondary gamma-rays with scattering angles greater than 90 degrees is significantly lower than that of the source beam. The equation for Compton scattering energy is:

$$E = \frac{E'}{1+\frac{E'}{0.511\ MeV}(1-\cos\theta)} \tag{2.1}$$

where E is the energy after the scatter, E' is the initial energy of the photon, and θ is the angle at which the photon travels after the scatter. The forward and backward scattering regions correspond to scattering angles of 0 to ± 90 and ± 90 to ± 180, respectively. For 2.14 MeV initial energy gammas, which is roughly the energy required to induce an NRF reaction in ^{239}Pu, these scattering regions have cutoff energies shown below.

$$E' = 2.143570\ MeV \tag{2.2}$$

$$E(\pm 90) = 0.412633\ MeV \tag{2.3}$$

$$E(180) = 0.228289\ MeV \tag{2.4}$$

Table 2-1 shows the ^{239}Pu NRF absorption and emission energies, which are seen to be well separated from the Compton back-scattered cutoff energies.

Table 2-1 Energies of interest for NRF reactions in 239Pu[37]

Isotope	Absorption (MeV)	Emission 1 (MeV)	Emission 2 (MeV)	Emission 3 (MeV)
^{239}Pu	2.143570	2.143550	2.135689	0.007861

As conveyed in the information presented above, using the backscattering regions pushes the Compton scatter energies far below the NRF emission energies. By reducing detector contributions from un-collided source photons and Rayleigh scattered photons,

and minimizing the energy region from Compton scatters, the NRF emission photons can be isolated from background/noise.

2.3 Analysis of Simulation Results

As a proof-of concept scenario, the geometry was tested using a spent nuclear fuel assembly with burn-up characteristics as specified in the NGSI-SF project.[35] This target consisted of a generic PWR fuel assembly that had a 4% initial ^{235}U enrichment and was burned for 45 gigawatt-days/metric ton of heavy metal (GWd/tHM) with no cooling time. These parameters resulted in a ^{239}Pu atom fraction of 0.151%. The spent fuel atom percentages that were used in the simulation are shown in **Table 2-2**. The fission products and the transuranics not included in the table were removed from the composition to reduce the computational time.

Table 2-2 Spent fuel assembly atom percentages for 0.15% 239Pu

Nuclide	^{16}O	^{238}U	^{235}U	^{236}U	^{239}Pu	^{240}Pu	^{241}Pu	^{242}Pu	^{238}Pu
Atom Percentage (% total)	67.777%	31.479%	0.233%	0.190%	0.151%	0.093%	0.043%	0.027%	0.027%

Using the geometry from ***Figure 2.1*** and the spent fuel atom percentages from **Table 2-2,** a detector response spectrum was obtained. For this case the detectors were sodium-iodide (NaI) crystals, and the detectors were placed in the backscattering position. The detector responses in this section were obtained through a pulse tally in the detectors. This detector type works by analyzing the deposited energy in the detector region for a given particle and all of the subsequent daughter particles.[37]. It is important to note that this tally type methodology does not model any of the efficiency reductions from the electronics. In an actual measurement scenario of a spent fuel assembly using real detectors, the peaks will not be as well defined as they are in the figure due to electronic noise and detection efficiency. The detector response is shown in ***Figure 2.2*** and the prominent features in the spectrum are labeled. One billion source particles were simulated to obtain this spectrum.

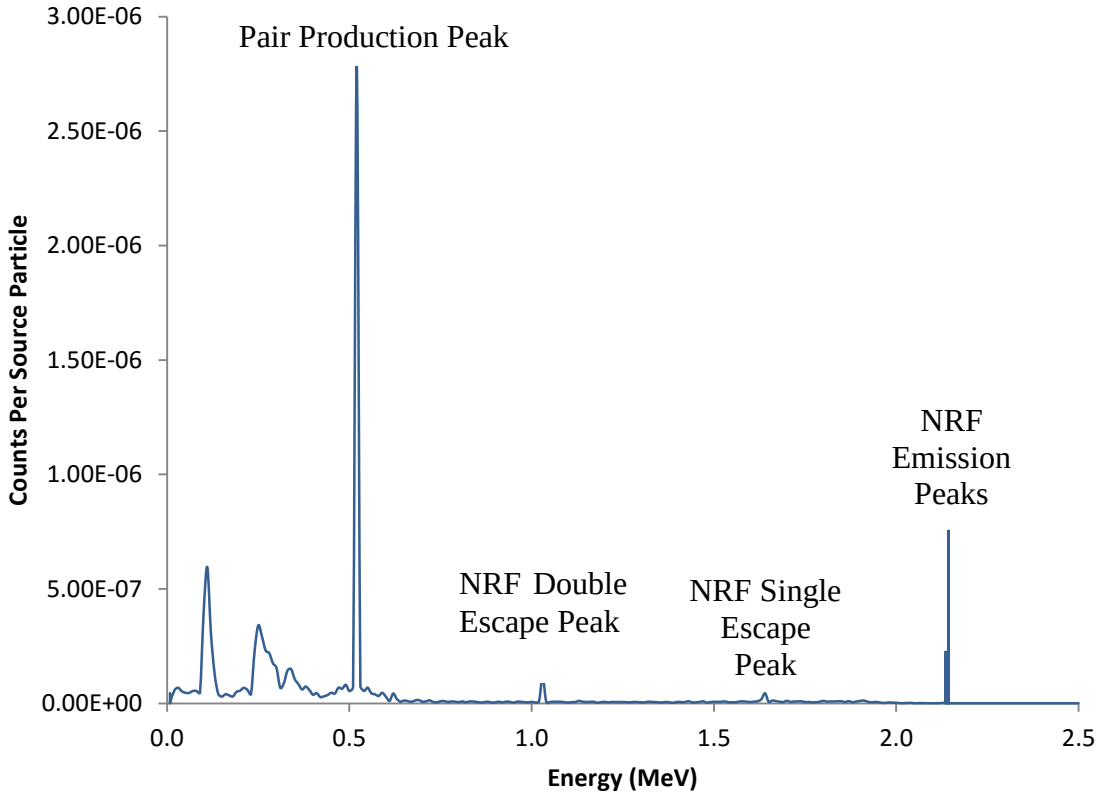

Figure 2.2 *Counts per source particle from witness piece detectors for 0.15% 239Pu atom fraction*

The initial observation of this data suggests that the application of the backscatter technique follows what was expected. There is little to no noise around the NRF emission peak energies. The closest significant source of noise is due to the photoelectric interactions in the detector material, labeled as escape peaks in the figure.

Once the results for a single ^{239}Pu percentage in a spent fuel assembly had been analyzed, the ^{239}Pu percentage was varied and the corresponding material in the spent fuel was adjusted. This adjustment was completed by increasing the ^{239}Pu percentage by the

desired amount while leaving the other nuclide percentages unchanged. The total atom fraction was then summed and the nuclide percentages were divided by the sum to re-normalize the atom fraction. This process will begin to provide unrealistic compositions at high ^{239}Pu levels, i.e. ^{239}Pu percentages of 50% and 90% in **Table 2-3;** however, the region of interest is in the <1% ^{239}Pu percentages, which is typical of spent fuel assembly values.[7,8]

Table 2-3 Spent fuel atom percentages for data points in ***Figure 2.3***

Data Point	^{16}O	^{238}U	^{235}U	^{236}U	^{239}Pu	^{240}Pu	^{241}Pu	^{242}Pu	^{238}Pu
0.15%	67.777%	31.479%	0.233%	0.190%	0.151%	0.093%	0.043%	0.027%	0.027%
0.30%	67.662%	31.425%	0.233%	0.189%	0.299%	0.093%	0.043%	0.027%	0.027%
0.50%	67.528%	31.363%	0.232%	0.189%	0.498%	0.093%	0.043%	0.027%	0.027%
0.72%	67.380%	31.294%	0.232%	0.188%	0.716%	0.092%	0.043%	0.027%	0.027%
1.5%	66.861%	31.053%	0.230%	0.187%	1.480%	0.092%	0.043%	0.027%	0.027%
3.0%	65.887%	30.600%	0.227%	0.184%	2.916%	0.090%	0.042%	0.027%	0.027%
5.0%	64.471%	29.943%	0.222%	0.180%	5.002%	0.088%	0.041%	0.026%	0.026%
50.0%	33.882%	15.736%	0.117%	0.095%	50.075%	0.046%	0.022%	0.014%	0.014%
90.0%	6.768%	3.143%	0.023%	0.019%	90.027%	0.009%	0.004%	0.003%	0.003%

By varying the ^{239}Pu concentration using this method, it would be possible to estimate the trend of the detector response as the ^{239}Pu concentration changed. ***Figure 2.3*** shows

the counts per source particle obtained by the detectors surrounding the witness piece which were obtained from COG simulations of the varying ^{239}Pu in **Table 2-3**. It is important to note that the counts per source particle results presented in the figure are only for photons emitted from NRF events in the witness piece. The reason for the smaller error bars at some data points is due to the difference in the number of particles simulated. An increased number of particles were simulated in the four data points near 1% ^{239}Pu concentration to obtain better resolution of the shape of the curve near the end of the flat region.

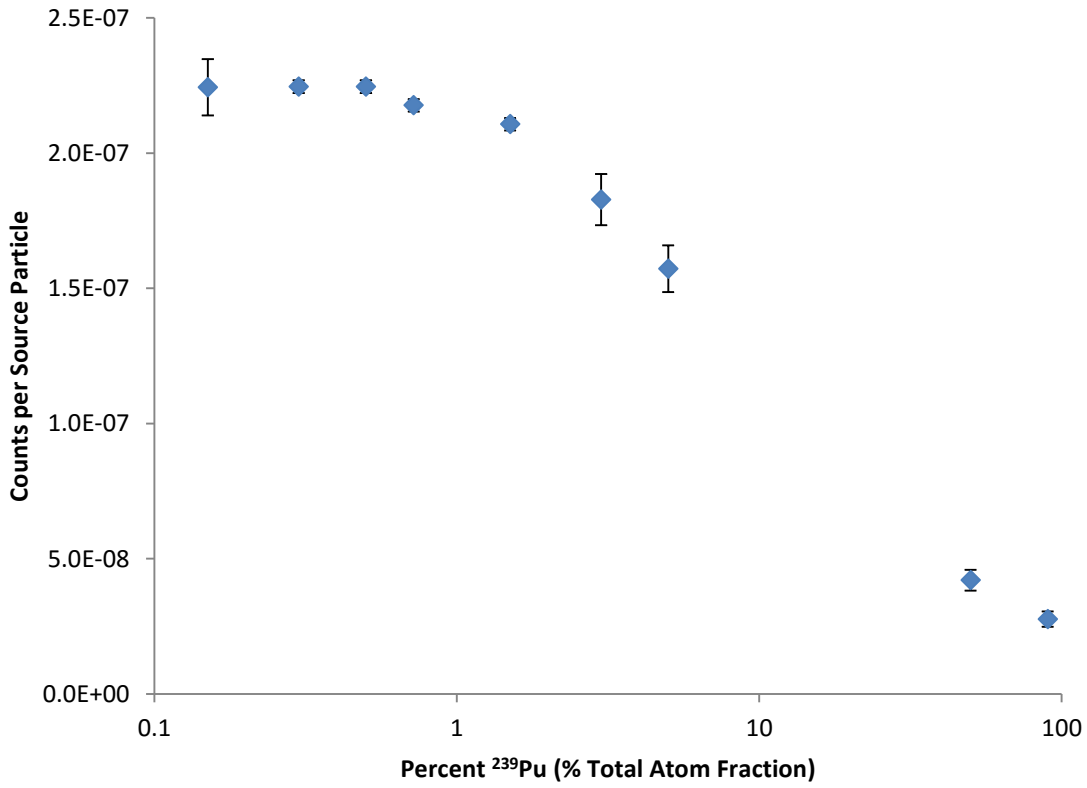

Figure 2.3 *Detector response across varying 239Pu for NRF emission photons*

As can be seen in ***Figure 2.3***, at ^{239}Pu concentrations greater than 1 atom percent the detector response in counts per source particle acts as expected. The counts per source particle should decrease exponentially as the amount of ^{239}Pu in the fuel assembly increases. ***Figure 2.4*** represents a side-view of the simulation configuration. In the figure I_o represents the number of photons emitted by the MEGa-Ray source, I_a represents the number of photons exiting the fuel assembly, and I_w represents the number of photons exiting the witness piece.

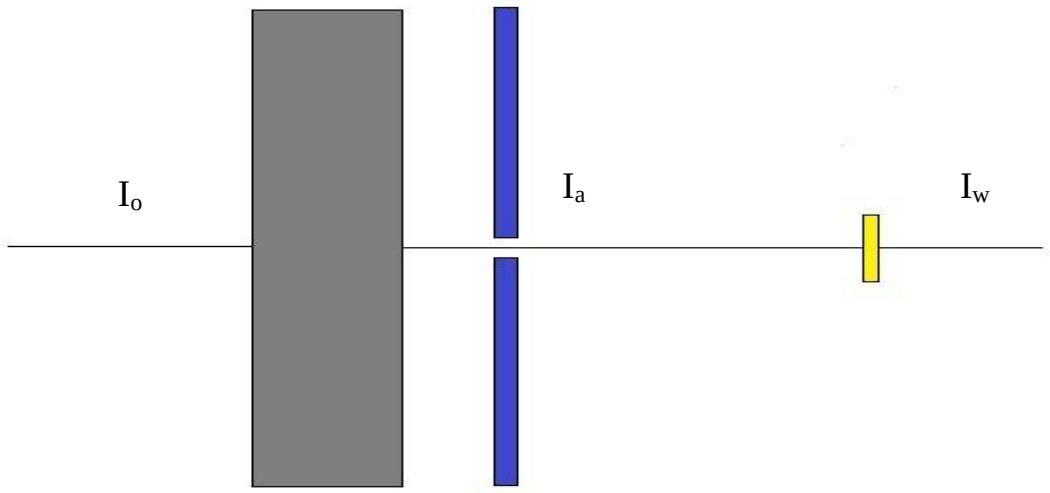

Figure 2.4 *Side view of geometric configuration for initial geometry simulations*

The relationships for linear attenuation through the fuel assembly and witness piece are shown in the equations below, where μ is the linear attenuation coefficient for NRF interactions in ^{239}Pu by photons with ~2.14 MeV energy and *x* is the thickness of the material:

$$I_a = I_o e^{-(\mu_a x_a)} \tag{2.5}$$

$$I_w = I_a e^{-(\mu_w x_w)} = \left[I_o e^{-(\mu_a x_a)}\right] e^{-(\mu_w x_w)} \tag{2.6}$$

By subtracting Equation 2.6 from Equation 2.5 it is possible to get the number of photons absorbed in the witness piece, ΔI_w:

$$\Delta I_w = I_a - I_w = I_o e^{-(\mu_a x_a)} - \left[I_o e^{-(\mu_a x_a)}\right] e^{-(\mu_w x_w)} \tag{2.7}$$

$$\Delta I_w = I_o e^{-(\mu_a x_a)}\left[1 - e^{-(\mu_w x_w)}\right] \tag{2.8}$$

In the simulations the witness piece remains unchanged as well as the thickness of the fuel assembly. As such it is possible to make the following simplifications to Equation 2.8, where C_n is a constant:

$$\Delta I_w = I_o e^{-(C_1 \mu_a)}[1 - e^{-C_2}] \tag{2.9}$$

$$\Delta I_w = C_3 I_o e^{-(C_1 \mu_a)} \tag{2.10}$$

Equation 2.10 shows the number of photons absorbed in the witness piece due to NRF interactions is only dependent on the linear attenuation coefficient for the fuel assembly. The linear attenuation coefficient is inversely proportional to the mean free path of the material, λ, and therefore directly proportional to the macroscopic cross-section, Σ, as seen in Equation 2.11:

$$N\sigma = \Sigma = \frac{1}{\lambda} = \frac{\int_0^\infty e^{-\mu x} dx}{\int_0^\infty x e^{-\mu x} dx} \tag{2.11}$$

Since the macroscopic cross-section is directly related to the linear attenuation coefficient the following holds true, where N_{239} is the number of ^{239}Pu atoms per unit volume in the assembly:

$$\Delta I_w = C_3 I_o e^{-(C_4 \Sigma_a)} \tag{2.12}$$

$$\Delta I_w = C_3 I_o e^{-(C_4 N_{239} \sigma_a)} \tag{2.13}$$

Equation 2.13 can be further simplified because the cross section for NRF reactions in ^{239}Pu does not change, since the reaction requires a very specific energy to occur. The resulting simplified equations shows that the number of NRF interactions in the witness piece is exponentially dependent on the number of ^{239}Pu atoms per unit volume in the spent fuel assembly as shown in Equation 2.14:

$$\Delta I_w = C_3 I_o e^{-(C_5 N_{239})} \tag{2.14}$$

There will be a geometric efficiency factor that must be accounted for due to the positioning of the detectors. The previous equations only go as far as to show the behavior of the number of NRF events occurring in the witness piece. Once an NRF event occurs, a slightly lower energy photon must be emitted; this photon is the relaxation photon that is equal to the incident photon energy minus the recoil energy of the nucleus. This emission is isotropic, and as such, the positioning of the detectors will cause a loss of detection efficiency. In addition, no detector is 100% efficient, so there will be additional loss of counts due to the detector efficiency. COG is able to account for the effects of

particle attenuation and geometric efficiency reductions. ***Figure 2.5*** shows a top and bottom comparison of the simulated NRF events in the witness piece per source particle and the analytically calculated NRF events in the witness piece per source particle, respectively.

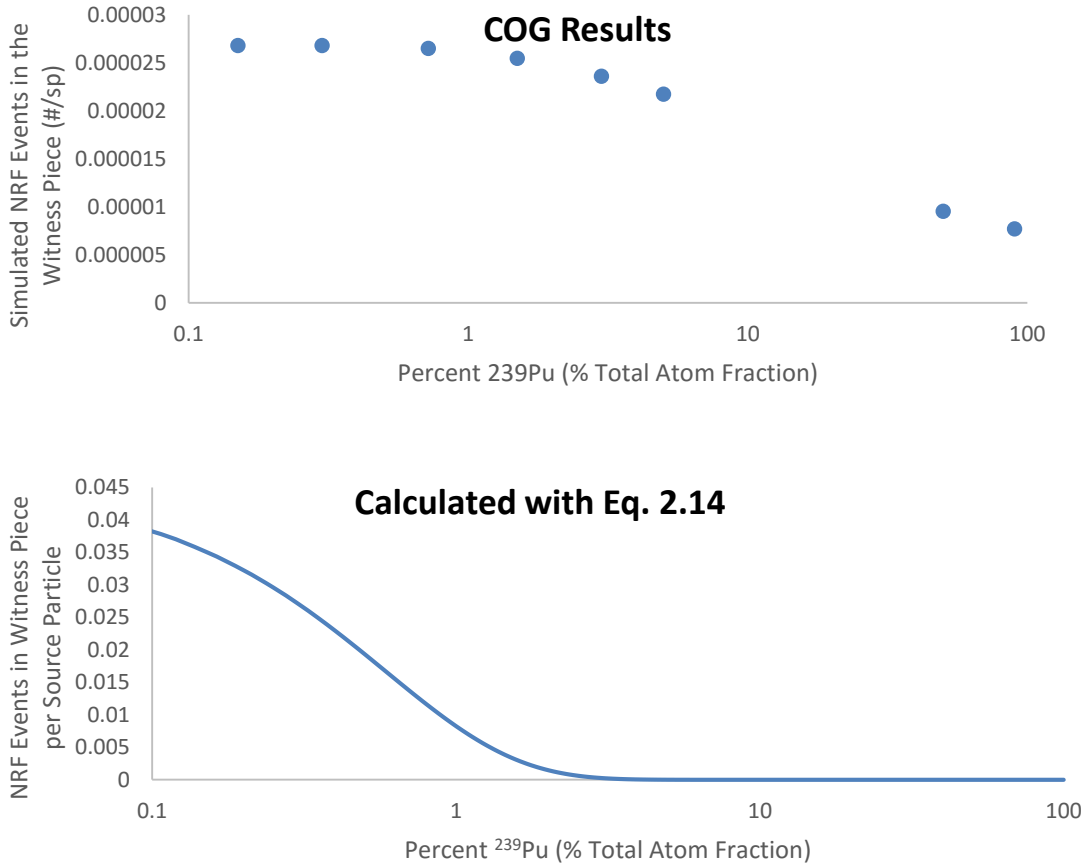

Figure 2.5 *Simulated counts per source particle in detectors (top) and calculated NRF events in the witness piece per source particle (bottom)*

The flattened region is present in the simulated case, but not the analytical case. However, as was previously stated, the trend of the simulated results greater than 1% ^{239}Pu

follow the expected exponential decay. If the region less than 1% ^{239}Pu had not flattened out it would be possible for the overall shape of the simulation results to match the calculated shape. It is important to note that the curve obtained through equation 2.14 is only a rough estimate of what happens in the fuel. The slope should be shallower in a more realistic case. This is because only ^{239}Pu was used, more specifically only NRF interactions in ^{239}Pu were included. There will be other competing reactions such as Compton and photoelectric that will affect the number of photons that are able to cause NRF. Also, there is the geometric simplification that the fuel is represented by a single block of material, and not individual fuel pins and their corresponding cladding. The cladding will also have competing reactions, which will decrease the number of photons that could cause NRF. These details should also be a strong reason why the simulated results have orders of magnitude less than the analytic equation values.

Figure 2.6 shows a zoomed plot of the low ^{239}Pu percent content region present in ***Figure 2.5***. The number of data points was increased using the same altering of the ^{239}Pu concentration that was previously presented.

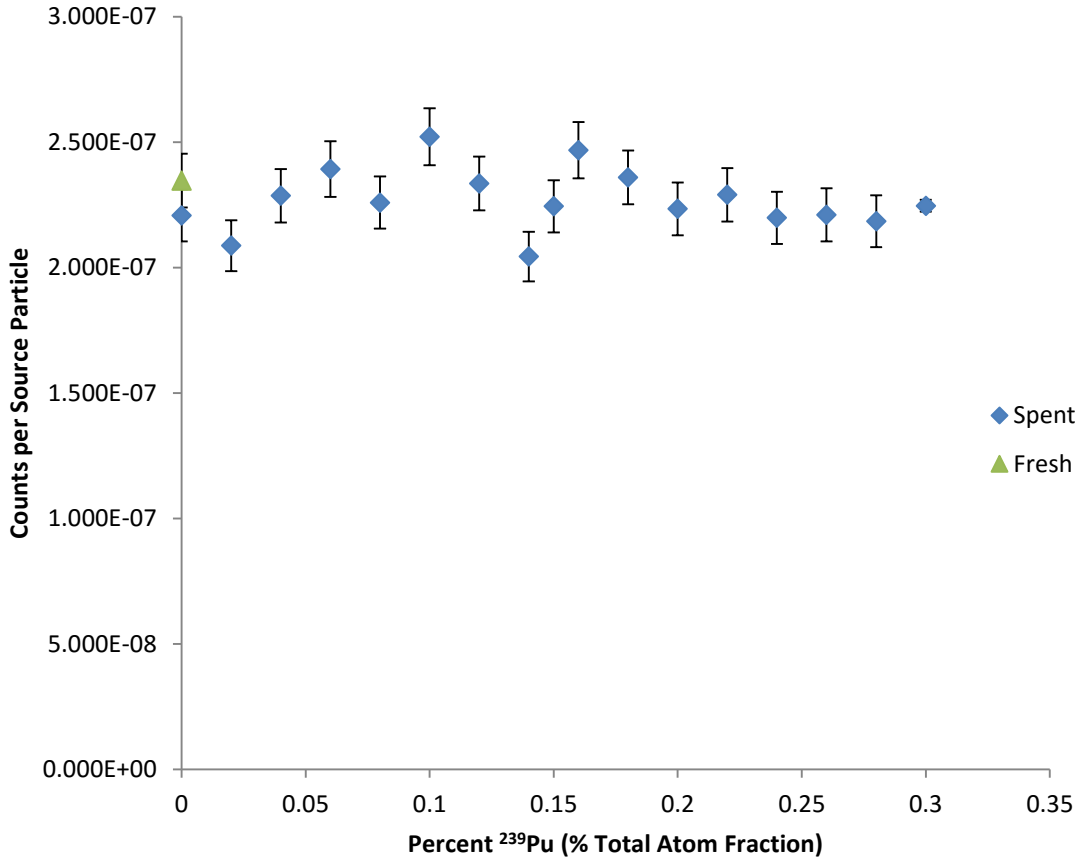

Figure 2.6 *Detector response for expanded low 239Pu concentrations*

Statistically, the data in ***Figure 2.6*** are indistinguishable. This is not logical because the data shows that having no ^{239}Pu, the fresh fuel data point, is statistically equivalent to having 0.3% ^{239}Pu. After various tests, the reason behind the flat region could not be identified.

2.4 Adjustment of Initial Geometry

The witness piece was modified from a foil geometry to a slug geometry. The concern was there were not enough NRF interactions happening in the thin foil witness piece and that this poor sampling was altering the results. The thicker slug target contained more gamma-ray mean free paths than a foil, thus providing more NRF interactions. The slug consists of a cylinder with a small radius but a large depth oriented so the flat faces are perpendicular to the source beam. This change was made, and the isotopic composition of the spent fuel assembly is shown in **Table 2-4** and the results from changing the witness piece geometry is shown in ***Figure 2.7***.

Table 2-4 Spent fuel assembly atom percent composition

Nuclide	^{16}O	^{238}U	^{235}U	^{236}U	^{239}Pu	^{240}Pu	^{241}Pu	^{242}Pu	^{238}Pu
Atom Percent (% total)	67.777%	31.479%	0.233%	0.190%	0.151%	0.093%	0.043%	0.027%	0.027%

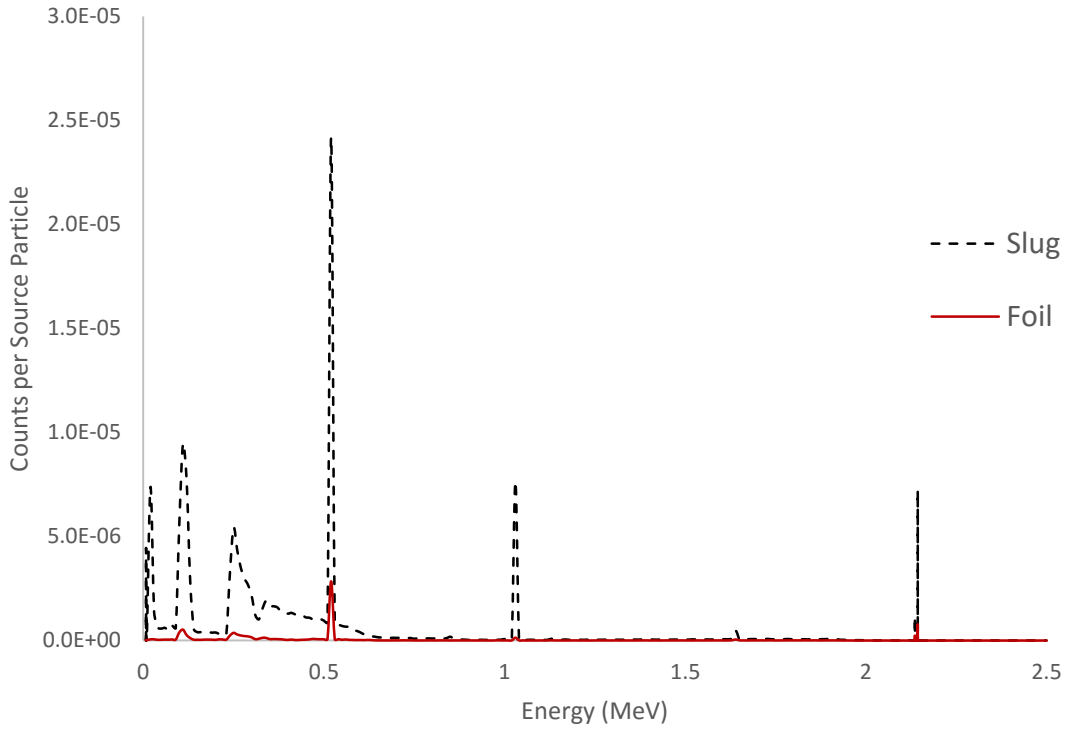

Figure 2.7 *Comparison detector response for witness piece as a foil and a slug for 0.15% 239Pu concentration*

As can be seen, the overall efficiency of the system was increased. By increasing the number of mean free paths in the witness piece, the number of NRF emissions increases, and as such the detector response increases. All other aspects of the geometry were held constant when compared to the initial geometry from ***Figure 2.1***. However, changing from a foil to slug did not result in any change in the shape of the detector response.

3. TEST GEOMETRIES

3.1 Overview

Based upon the unexplained behavior in the initial results, simple geometries were created to determine if the code behaved as expected for material mixtures. For these simple geometries, a cube with dimensions of 1 cm by 1 cm by 1 cm with a mono-energetic, pencil beam of photons incident on it was modeled. COG outputs the number of event interactions and the type of interaction in every declared region. Using this output allows for any potential user error from detector tallies to be eliminated. The geometry is shown in ***Figure 3.1***.

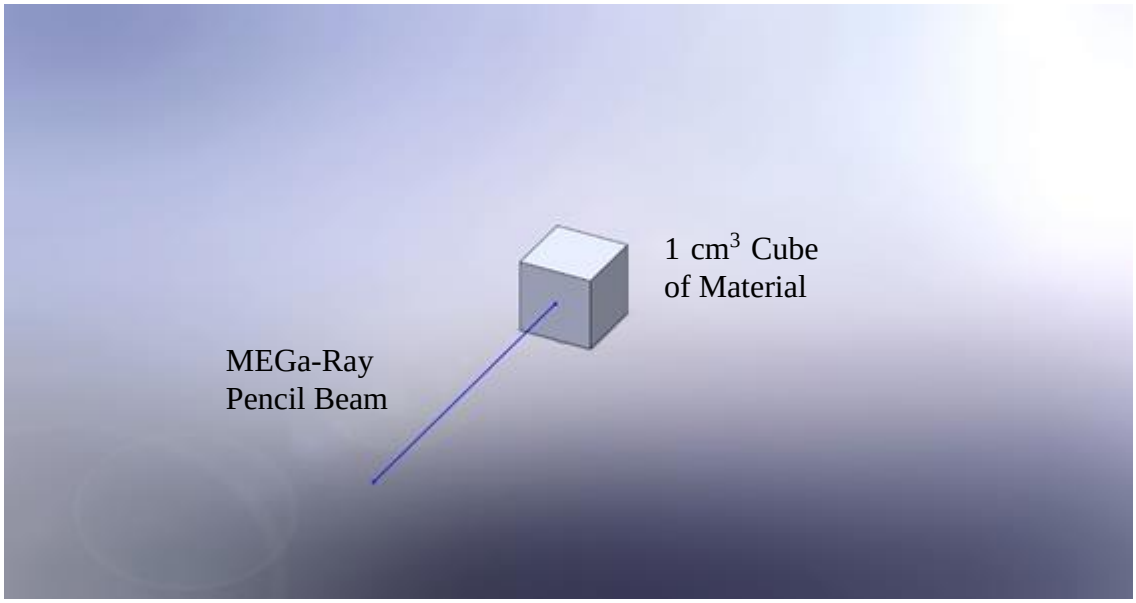

Figure 3.1 *Geometry for block test simulations*

This is the general geometry that will be used in all of the simulations in the following sections; however, the depth of the cube will be altered in Section 3.3 and the depth and density will be altered in Section 3.5. The specific geometric and physics parameters can be found in **Appendix B** for all of the associated sections.

3.2 ^{239}Pu and ^{238}U Block Test

The composition of this cube consisted of a mixture of only ^{239}Pu and ^{238}U. Since the atomic number and therefor the number of electrons per atom are similar there should be a small difference between Compton and photoelectric events when changing the ^{239}Pu percentage. The number of events for the NRF, Compton scattering, photoelectric, and total events in the cube were obtained and compared across varying concentrations of ^{239}Pu. ***Figure 3.2*** through ***Figure 3.5*** show this data for NRF reactions, Compton reactions, photoelectric reactions, and total reactions, respectively. The uncertainty bars on the data points are not visible because of how small the values for the errors were. **Table 3-1** shows the data point's atomic percentages for the results in ***Figure 3.2*** through ***Figure 3.5***.

Table 3-1 Atom percentages for 239Pu and 238U block tests

Data Point	Percent ^{239}Pu (atom %)	Percent ^{238}U (atom %)
1	0.00	100.00
2	0.25	99.75
3	0.50	99.50
4	0.75	99.25
5	1.00	99.00
6	1.25	98.75
7	1.50	98.50
8	2.00	98.00
9	2.50	97.50
10	3.00	97.00
11	5.00	95.00
12	15.00	85.00
13	30.00	70.00
14	50.00	50.00

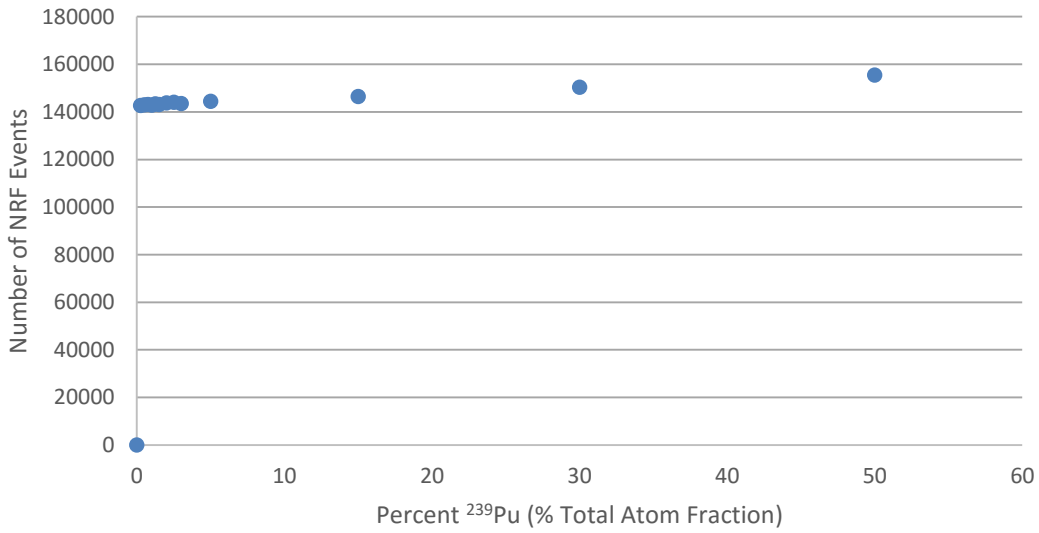

Figure 3.2 *Number of NRF events in a block of spent nuclear fuel 1.0 cm thick across varying 239Pu concentrations*

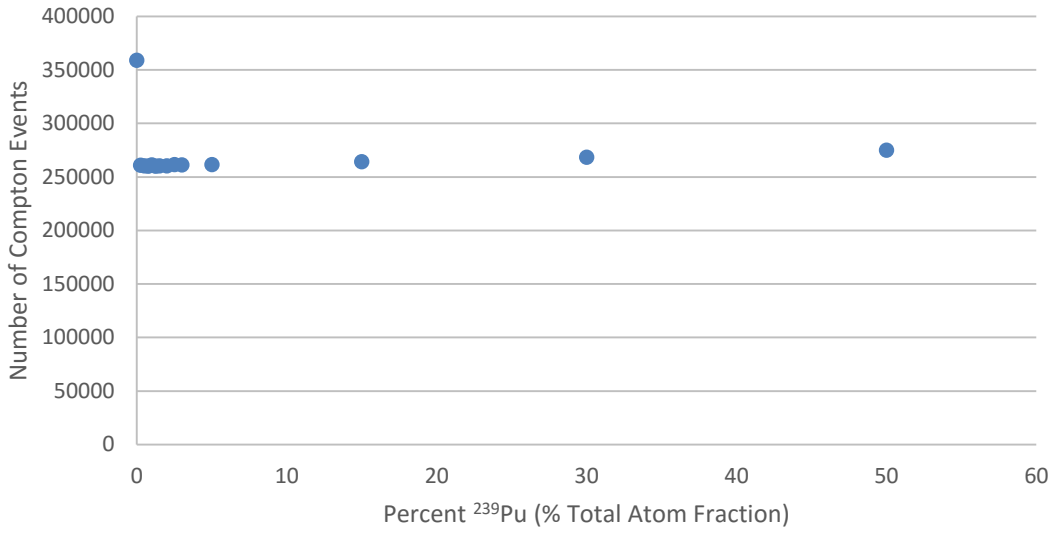

Figure 3.3 *Number of Compton events in a block of spent nuclear fuel 1.0 cm thick across varying ^{239}Pu concentrations*

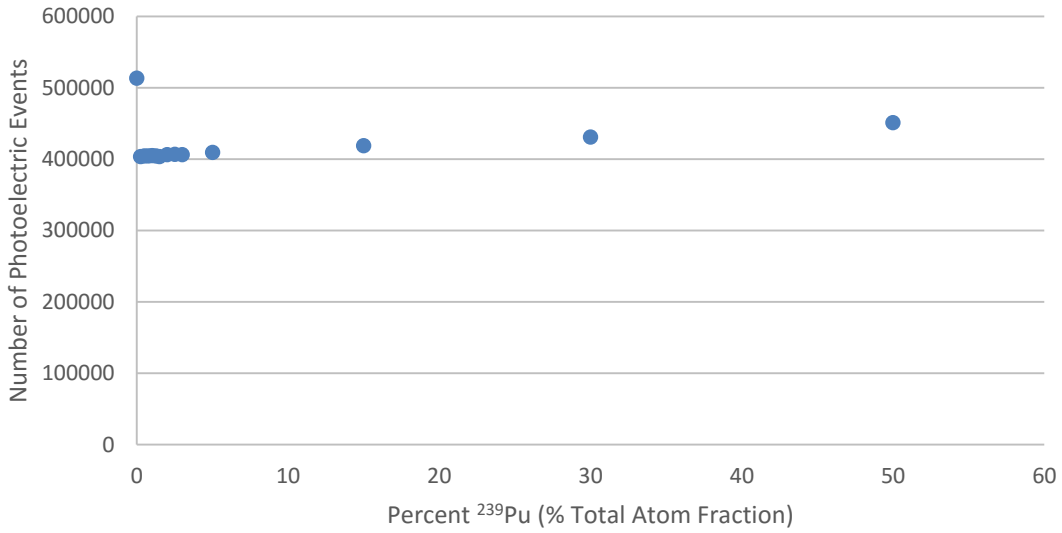

Figure 3.4 *Number of Photoelectric events in a block of spent nuclear fuel 1.0 cm thick across varying ^{239}Pu concentrations*

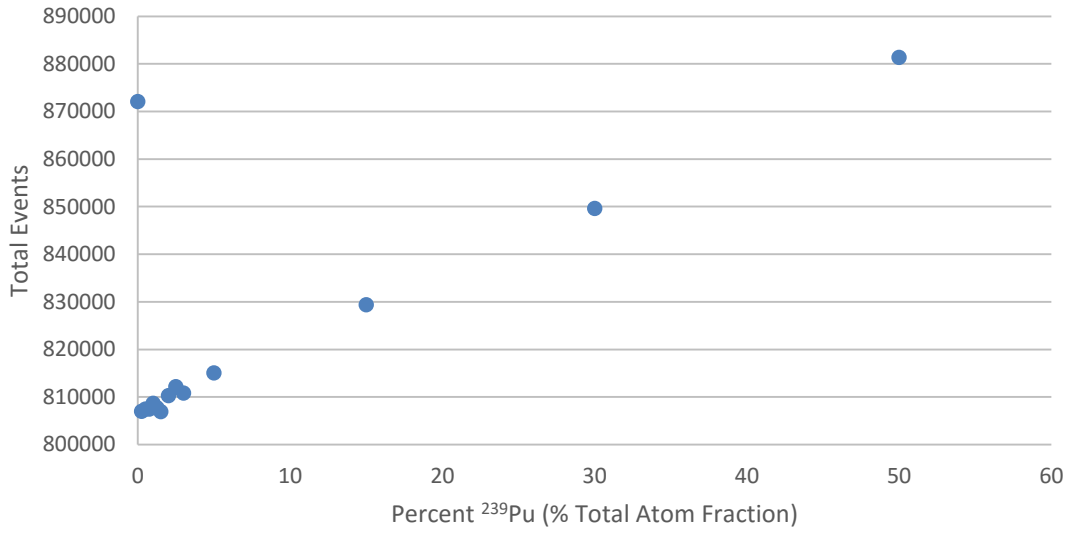

Figure 3.5 *Number of total events in a block of spent nuclear fuel 1.0 cm thick across varying ^{239}Pu concentrations*

The figures show there is a discontinuity in the number of events from zero ^{239}Pu to any amount of ^{239}Pu. This is shown by the prompt jump of the number of NRF events, and the prompt drops of the Compton, Photoelectric, and total events. However, once the jump had occurred, the general trend of the three event types continued as expected; any increase in ^{239}Pu caused a proportionate increase in the number of events in the block for all of the reaction types.

Figure 3.6 shows the number of NRF events in the cube as the concentration of ^{239}Pu is brought to extremely low values. There are error bars on these data points, however they are not visible due to the small values.

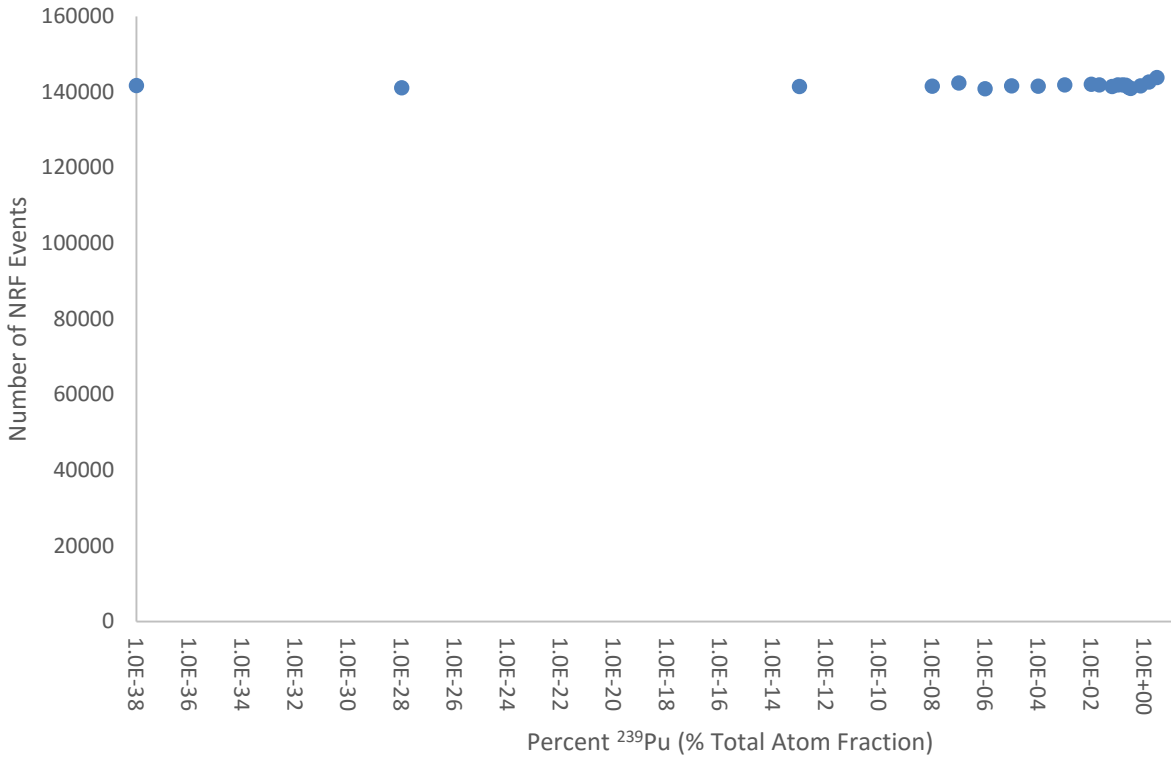

Figure 3.6 *Number of NRF events occurring in a cube with a volume of 1 cm3 across varying 239Pu concentrations*

The figures show there is a discontinuity in the number of events from zero ^{239}Pu to any amount of ^{239}Pu. This is shown by the prompt jump of the number of NRF events, and the prompt drops of the Compton, Photoelectric, and total events. However, once the jump had occurred, the general trend of the three event types continued as expected; any increase in ^{239}Pu caused a proportionate increase in the number of events in the block for all of the reaction types.

3.3 Pure ^{239}Pu Block Tests

The composition of the sample material was further simplified to identify the cause for the irregularities in the results. The material was reduced to pure ^{239}Pu, and the depth of the cube (i.e., along the axis of the gamma ray beam) was adjusted to alter the amount of ^{239}Pu transited by the gamma beam. The results are shown in ***Figure 3.7***. The error bars on the data points are not visible due to the small values of error on each point.

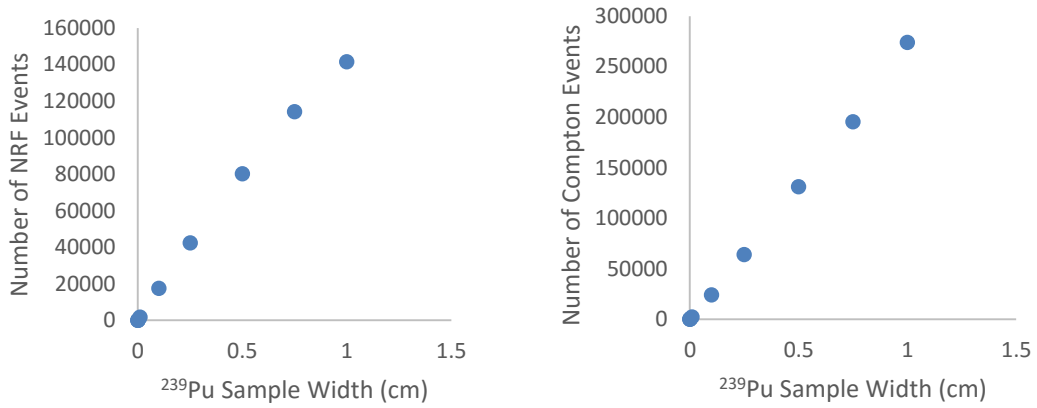

Figure 3.7 *Number of NRF (left) and Compton (right) events in a sample of pure 239Pu across varying depths*

Based on the plots in ***Figure 3.7*** above, it is evident that COG behaves as expected for small samples of pure ^{239}Pu that are not foils. This result is logical because as the sample

depth increases, the number of ^{239}Pu atoms that can interact with the beam increases, therefore increasing the number of NRF and Compton events in the block in a linear fashion.

3.4 Block of ^{239}Pu and ^{16}O Mixture

Figure 3.8 shows a 1 cm by 1 cm by 1 cm cube of ^{239}Pu and ^{16}O mixture. ^{16}O was chosen because the cross-sections for Compton and Photoelectric reactions are significantly lower than those for ^{239}Pu. In addition, oxygen is always found in spent nuclear fuel because the fuel is, most commonly, inserted as UO_2 for PWRs. Similar to previous figures the error bars on the data points are not visible because of the small values. **Table 3-2** contains the atom percentages for ^{239}Pu and ^{16}O for ***Figure 3.8***.

Table 3-2 Atom percentages for 239Pu and 16O block tests

Data Point	1	2	3	4	5	6
Percent ^{239}Pu (atom %)	0.5	1.0	1.5	2.0	2.5	3.0
Percent ^{16}O (atom %)	99.5	99.0	98.5	98.0	97.5	97.0

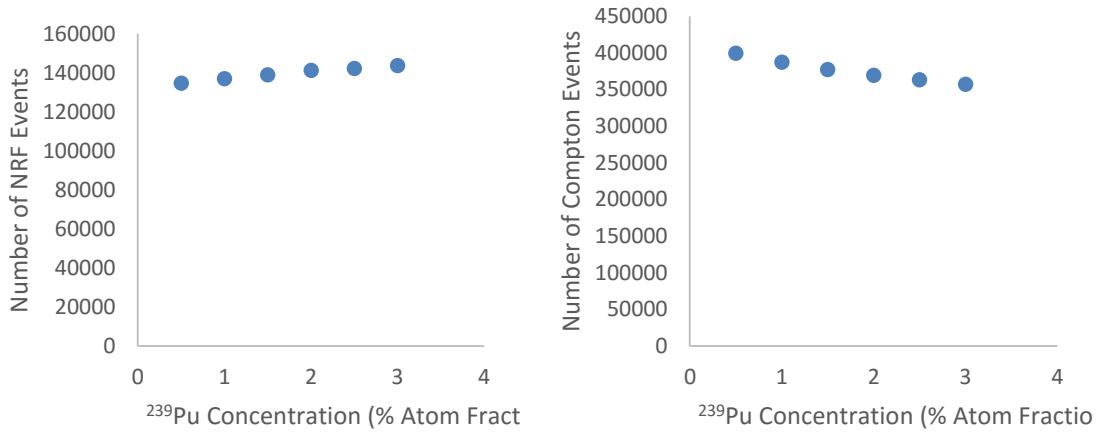

Figure 3.8 *Number of NRF (left) and Compton (right) events in a sample of 239Pu and 16O*

A similar trend to that encountered with the ^{239}Pu and ^{238}U isotopics, in section 3.1, can be seen. This trend shows a large amount of NRF events despite having a low amount of ^{239}Pu in sample. Even though the materials in ***Figure 3.8*** have much less ^{239}Pu - single digit percentages compared to pure samples - the number of NRF events is comparable to ***Figure 3.7*** (the pure Pu case) in the previous section. For a volume of 1 cm^3, the number of NRF events from the Pu and O mixture should be, at most, 3% of the pure ^{239}Pu sample at the same volume. Specifically, the number of NRF events for the Pu and O mixture should be less than ~4,200 because it only has 3% of the number of ^{239}Pu atoms that the pure 1 cm sample has, which had ~142,000 NRF events.

3.5 Photon Splitting in COG

Using energy deposition instead of the number of events in a material was identified as a possible solution to the anomalous count rates at low Pu concentrations. The theory

behind this proposal was that, in COG, when a photon that could possibly cause an NRF event reaches a material with an NRF cross-section, the particle is split. A portion of this particle is transported as it normally would be; however, the other portion is forced to undergo an NRF reaction. When a particle undergoes an NRF interaction, the amount of energy it would normally deposit is multiplied by the weight of the particle, which is conserved during the previous splitting process. This approach is valid because if the two weights of the particles post splitting were summed, the value would equal the original particle weight. Due to this forced splitting, the number of NRF interactions in any material consisting of more than one nuclide, will be inflated but the energy deposited by NRF interactions will be correct due to the conservation of particle weight. It is clear that the number of NRF events being reported in the output is incorrect. However, without having access to the source code the theory that energy deposition is handled correctly can only be tested by analyzing the energy deposition reported through the COG output file. In addition the weight of each split particle is unknown, without examining the source code, causing it to be difficult to create an analytical analysis of the results. ***Figures 3.9*** and ***3.10*** compare NRF (first) and Compton (second) energy deposition for various densities and thickness of the block geometry.

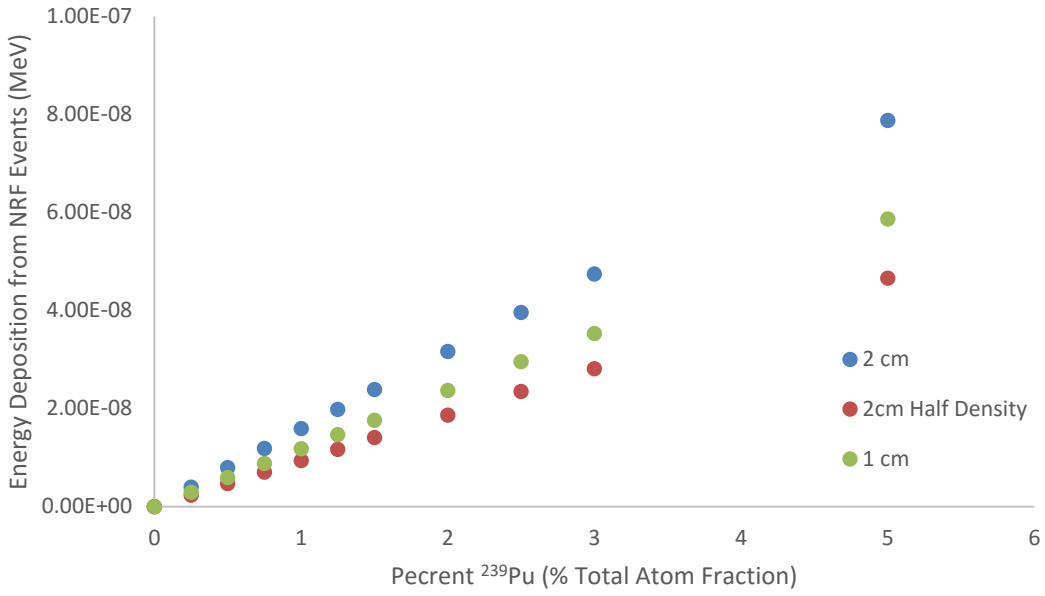

Figure 3.9 *Comparison of NRF energy deposition for a sample of 239Pu and 238U*

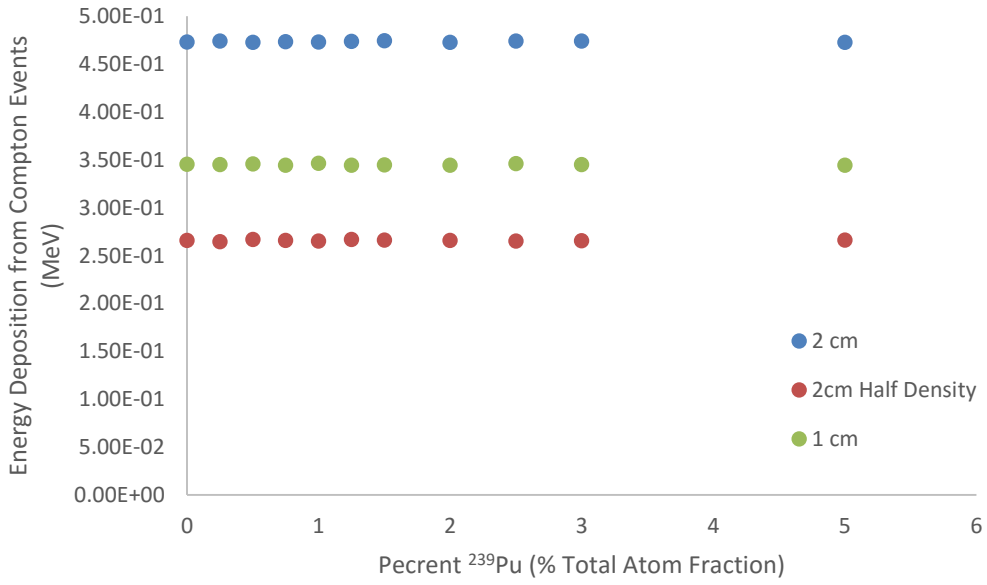

Figure 3.10 *Comparison of Compton energy deposition for a sample of 239Pu and 238U*

The previous figures demonstrate that, even for the case of a non-pure-Pu material, by using energy deposition to monitor the NRF events in the region of interest, the expected trend occurs. However, there is still a discrepancy in the energy deposition between geometries. By halving the density of a 2 cm depth sample, the energy deposition is not halved, despite the ^{239}Pu concentration in the block being halved. It is expected that halving the density of a 2 cm by 1 cm by 1cm block should result in extremely similar values for a 1 cm by 1 cm by 1 cm block of the original density for a given ^{239}Pu percentage. As can be seen in ***Figure 3.9*** and ***Figure 3.10***, this is not the case. The following equations prove that the assertion that halving the density but doubling the depth results in the same number of mean free paths for NRF reactions. Where λ is the mean free path, μ is the linear attenuation coefficient, x is the depth of the block, Σ is the macroscopic cross-section, N is the number of ^{239}Pu atoms per unit volume, σ is the microscopic cross-section, N_A is Avogadro's number, and M is the molar mass of ^{239}Pu.

$$\lambda = \frac{\int_0^\infty x e^{-\mu x} dx}{\int_0^\infty e^{-\mu x} dx} = \frac{1}{\mu} \tag{3.1}$$

$$\mu = \Sigma = N\sigma = \frac{\rho N_A \sigma}{M} \tag{3.2}$$

Combining Equations 3.1 and 3.2 result in the following relationships, where the subscripts 1 and 2 correspond to the depth of the blocks in cm:

$$\lambda_1 = \frac{M}{\rho_1 N_A \sigma} \tag{3.3}$$

$$\lambda_2 = \frac{M}{\rho_2 N_A \sigma} \tag{3.4}$$

Since the density of the 2 cm block is half of the 1 cm block the following relationship is true:

$$\lambda_2 = \frac{M}{\frac{1}{2}\rho_1 N_A \sigma} \tag{3.5}$$

$$\lambda_2 = \frac{2M}{\rho_1 N_A \sigma} = 2\lambda_1 \tag{3.6}$$

The number of mean free paths in the blocks is shown in Equation 3.7 below:

$$\#\ of\ mfps = \frac{x}{\lambda} \tag{3.7}$$

$$\#\ of\ mfps_1 = \frac{x_1}{\lambda_1} = \frac{1\ cm}{\lambda_1} \tag{3.8}$$

$$\#\ of\ mfps_2 = \frac{x_2}{\lambda_2} = \frac{2\ cm}{2\lambda_1} = \frac{1\ cm}{\lambda_1} \tag{3.9}$$

By comparing Equation 3.8 and 3.9 it is evident that the number of mean free paths in the material is equal. If the number of mean free paths is the same for the two blocks, the energy deposited in the 2 cm half density case should be the same as the 1 cm full density case. This is because the energy deposition per NRF reaction is a constant. The behavior of the Compton data should be equal for the two cases as well. Changing the density of a constant depth block results in the expected halving of the NRF energy deposition. However, when the depth of the block is reduced from 2 cm to 1 cm there is a loss of less than half of the NRF energy deposition, which is not expected. It is important to note that when density is held constant and the depth is held constant the overall trend of the deposition matches to what is expected: a linear increase in NRF energy deposition at low plutonium amounts, and a constant energy deposition for Compton. In the case of the fuel

assembly system, the depth of the fuel assemblies remains unchanged; the only thing that is being changed is the concentration of plutonium, which was shown to trend properly in this test case.

4. ENERGY DEPOSITION CORRECTION RESULTS

4.1 Overview

It was demonstrated in section 3.5 that using the energy deposition methodology for estimating NRF counts in constant density and target depth cases does provide useful results. Based on this success, the initial geometry was altered to use a witness slug and energy deposition. By using the energy deposition in the witness piece and the average energy deposited per NRF event, it is possible to calculate the number of NRF events occurring in the witness piece. Since the detectors will only be exposed to events happening in the witness piece, the number of NRF events in the witness piece will be directly proportional to the counts in the detectors. The input file was split in half - the first portion consisted of transporting the source photons through the fuel pins and collimator and the second portion took the collimated source and transported it to the witness piece. For this case the detectors were ignored, since the major fundamental difference between NRF events occurring in the witness piece and the NRF emission photons tallied by the detector is the geometric efficiency of the detector positions. Focusing purely on the number of events in the witness piece allows COG to rely completely on built-in fundamental nuclear interactions, without any possibility of introducing user interference by using a tally to obtain the results. This approach is valid because it was shown in section 3.3 that COG properly reports the number of NRF events occurring in a pure sample of ^{239}Pu, which the witness piece is.

4.2 Corrected Events in Fuel Assembly

The spent fuel assembly was the first focus of using energy deposition to determine the correct number of NRF events. If the overall trend across the assembly did not match what was expected, then the changes would have had no influence on the witness piece results. This lack of a change would be due to the relationship between the number of NRF events in the witness piece and the cross section of the assembly previously shown in Equation 2.10. ***Figure 4.1*** shows the energy deposition in the spent fuel assembly; the values consist of a sum across all of the individual fuel pins.

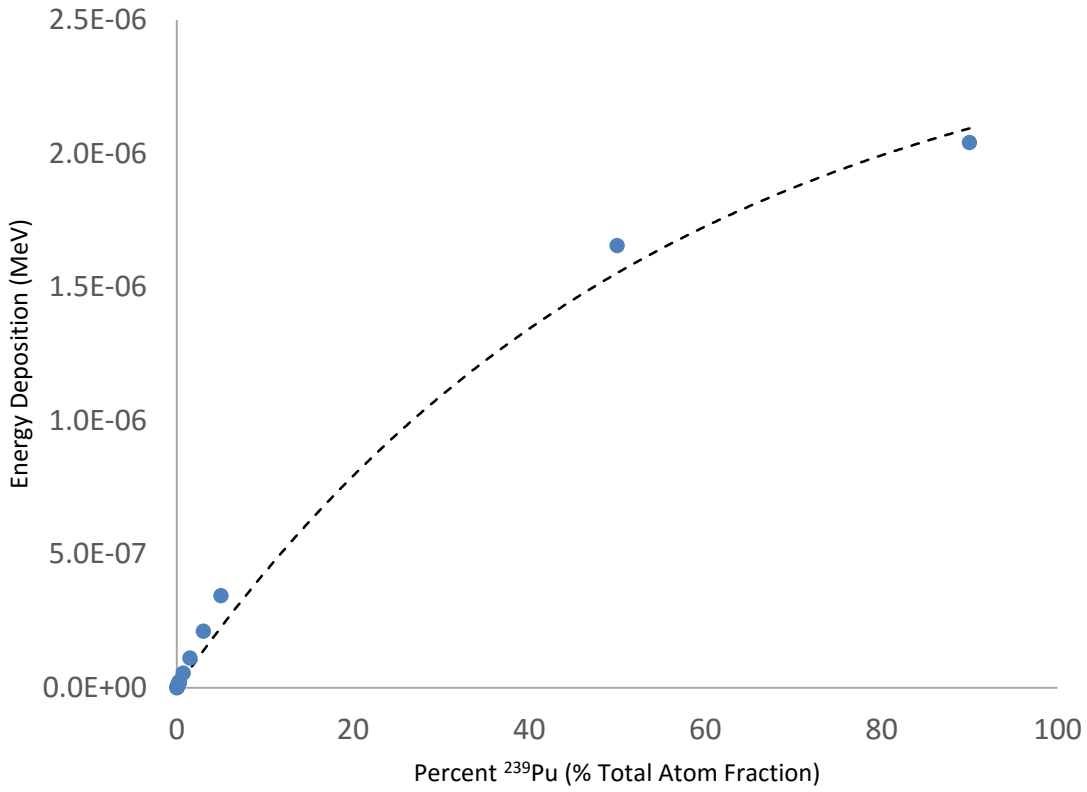

Figure 4.1 *Energy deposition from NRF reactions inside of the spent nuclear fuel assembly*

The black dotted line represents an exponential fit to the data points. As can be seen, the line does not fit the data as well as it should. Equation 4.1 shows the formula used for the fitting, where C is a fitting constant, dE is the energy deposition per NRF event, N_{239} is the atom density for ^{239}Pu, σ is the microscopic cross-section for NRF in ^{239}Pu, and x is the width of the fuel assembly.

$$E = CdE(1 - e^{-N_{239}\sigma x}) \tag{4.1}$$

One proposed reason for the difference between the data and the fitting curve is that the energy deposition is a function of more than one exponential. However, without access to COG's source code it is not possible to pursue this theory.

The energy that is deposited per NRF interaction is 20.635 eV according to documentation provided by LLNL.[37] By dividing the values in the figure above by this constant and then multiplying by the number of particles run, it is possible to get a "corrected" number of NRF events in the material. Upon completing this calculation, the resulting data was compared to the data obtained from the initial test case; this comparison is shown in the figure below.

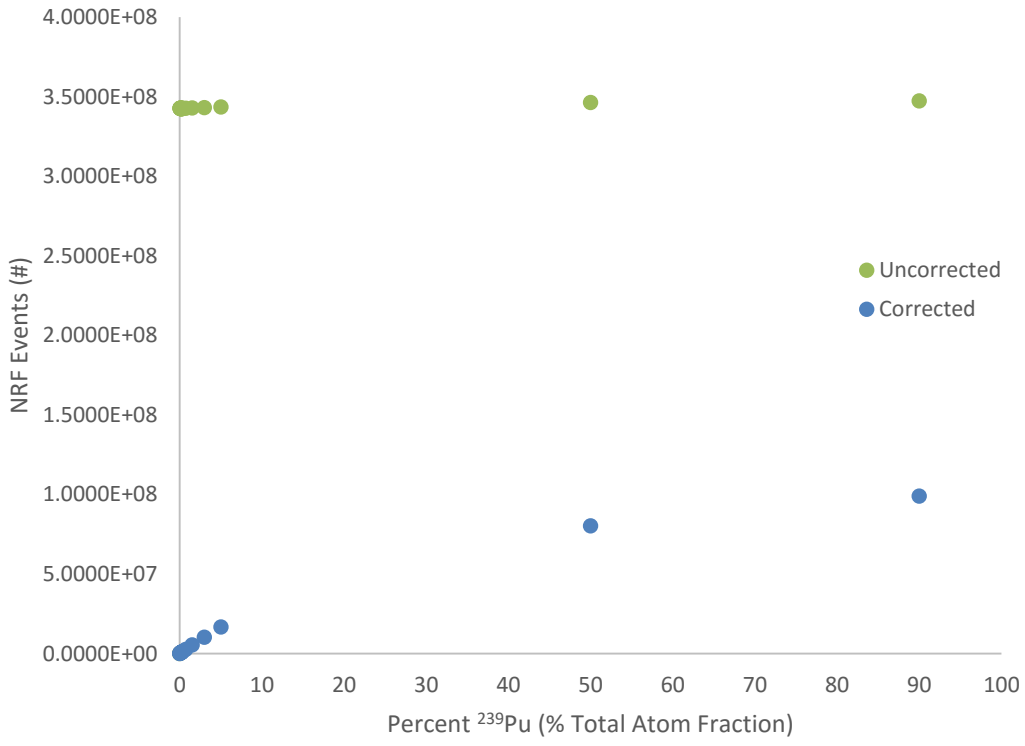

Figure 4.2 *Comparison of NRF events in a spent nuclear fuel assembly*

There is a dramatic difference between the number of NRF events occurring in the spent fuel assembly reported by COG and what is calculated through the energy deposition corrections. This difference between the two methods of obtaining the number of NRF events lends more credence to the theory that the reported number of NRF events in any region was inflated due to the photons being split and forcing collisions. This initial result showed promise, as it was expected that a similar trend could be found in the detector response.

4.3 Corrected Events in Witness Piece

The photons obtained after collimation were transported to the witness slug. ***Figure 4.3*** shows the number of NRF events occurring in the witness piece as a function of ^{239}Pu concentration in the fuel assembly.

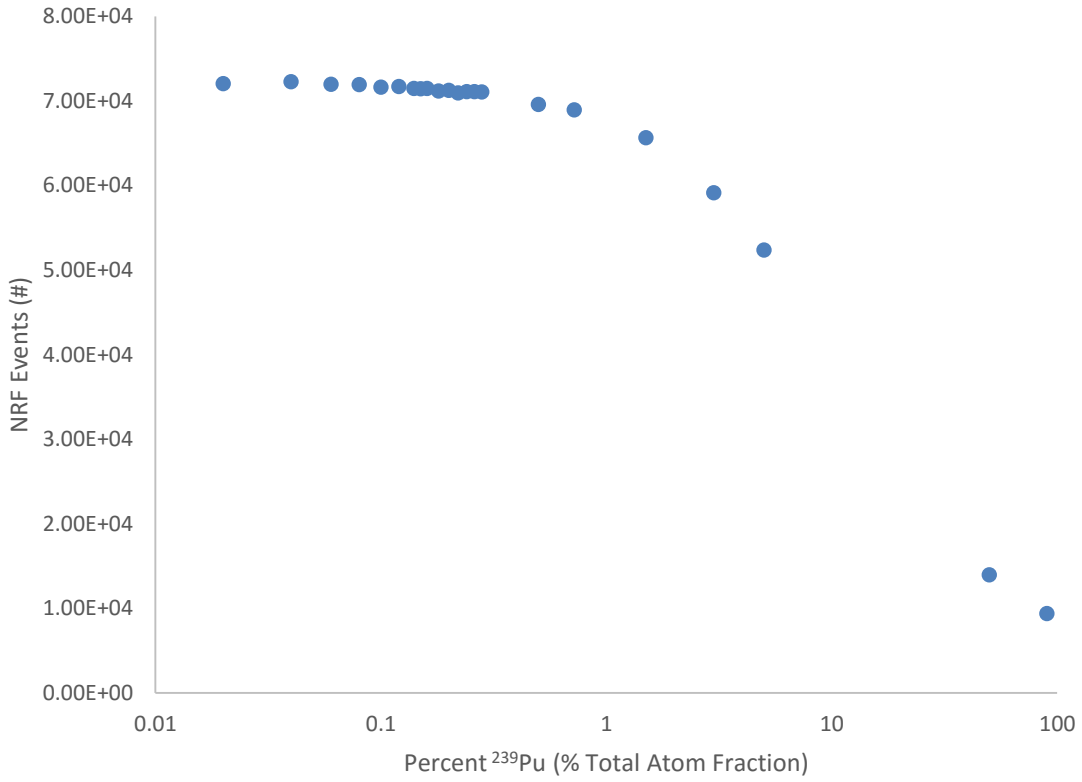

Figure 4.3 *Corrected number of NRF events in the witness piece*

The results in the figure above underwent the same mathematical changes, from energy deposition to number of events, as occurred in the previous section. Unfortunately, using the energy deposition in the spent fuel assembly and the witness piece, the overall shape of the curve remained unchanged. There is still an unexpected flat region at low ^{239}Pu concentrations. However, when using the energy deposition corrections the point at which the flattening turns over is more resolved than in the initial data. Further investigation of this region should be conducted to determine the source of the flattening.

Ignoring the flat region at low ^{239}Pu concentrations, i. e. <1% ^{239}Pu, it is possible to see that a large portion of the concentrations could be resolved from one another. Of most interest is the region following the elbow in the curve, the > 1% ^{239}Pu region. This is the Pu concentration found in fresh and spent Mixed OXide fuels (MOX). As a result, the NRF technique has the potential to be used to quantify plutonium in MOX fuel in LWR assemblies.

5. FINDINGS

From the first set of simulations it was evident that there was an unexplainable feature at low ^{239}Pu percentages, less than 1% ^{239}Pu; however, once the concentration of ^{239}Pu exceeded 1% the shape of the results seemed to match what was expected. In an attempt to remove the unexpected flattening of the results at low ^{239}Pu concentrations, the geometry of the witness piece was altered to be a slug instead of a foil. This change to the witness piece geometry caused an increase in the overall detection efficiency but did not remove the flattened region below 1% ^{239}Pu.

It was demonstrated that for a block of pure ^{239}Pu the number of NRF events in the block increased linearly as the depth of the block increased. Once the material was complicated through the addition of either ^{238}U or ^{16}O the code predicted an abrupt jump in the number of NRF events when the percentage of ^{239}Pu was non-zero. This anomaly was attributed to COG's forced splitting of the photons that were capable of inducing an NRF interaction. By using energy deposition in the regions instead of the number of events reported by COG it is possible to eliminate the anomalous prompt jump.

The energy deposition approach was carried over to the spent fuel assembly geometry, where it was shown again that the number of NRF events in the fuel assembly was being inflated. By using energy deposition to calculate the number of NRF events occurring in the witness piece it was possible to get a more detailed shape of the flattening at low ^{239}Pu percentages. Unfortunately, the flattened region still existed, but it was possible to identify the point at which the flattening occurred, ~1% ^{239}Pu.

6. CONCLUSIONS

In this work, the capability of NRF to quantify ^{239}Pu in Pressurized Water Reactor (PWR) spent nuclear fuel assemblies was assessed. Overall, high energy, mono-energetic gamma-ray (MEGa-Ray) beams could be useful for determining ^{239}Pu concentrations above roughly 1% through the use of Nuclear Resonance Fluorescence (NRF). Both the initial and final data show this. As a result, this technique should be able to determine the difference between various fresh and spent Mixed OXide (MOX) fuel assemblies. This is because both fresh and spent MOX fuels have higher ^{239}Pu concentrations than spent Pressurized Water Reactor fuel. However, due to the unexplained flattening of the simulation results for low ^{239}Pu concentrations, less than 1% ^{239}Pu, the ability to discriminate the ^{239}Pu content in Pressurized Water Reactor (PWR) fuel cannot be assessed. The vast majority of assemblies that are discharged from nuclear reactors will fall into this flat region. As such, the reason for this data flattening needs to be determined before final judgement on the application of Nuclear Resonance Fluorescence (NRF) to quantify ^{239}Pu in spent nuclear fuel can be made.

REFERENCES

[1] G.P. De Beer, A Compton Scatterer as a Source of Mono-Energetic Gamma Rays, Nucl. Instruments Methods. 78 (1970) 13–18.

[2] IAEA, The structure and content of agreements between the Agency and states required in connection with the Treaty on the Non-Proliferation of Nuclear Weapons, 153 (1972).

[3] O.O.T.A. US Congress, Nuclear Safeguards and the International Atomic Energy Agency, At. Energy. (1995) p. 11. doi:OTA-ISS-615.

[4] International Atomic Energy Agency, IAEA Safeguards Glossary, (2001) 23.

[5] N.S.S. and P. Institute, Nuclear Safeguards Education Portal, (n.d.). http://nsspi.tamu.edu/nsep/courses/the-nuclear-fuel-cycle/introduction/material-definitions/material-definitions,-part-1 (accessed July 23, 2015).

[6] USNRC, Pressurized Water Reactor (PWR) Systems, Manual, React. Concepts Water, Press. Syst. React. (2011) 28.

[7] B.K. Castle, S.A. Hoiland, R.A. Rankin, J.W. Sterbentz, Plutonium Discharge Rates and Spent Nuclear Fuel Inventory Estimates for Nuclear Reactors Worldwide, INL/EXT-12-27150 (2012).

[8] Iaea, Nuclear Fuel Cycle Simulation System (VISTA), Tecdoc-1535. (2007).

[9] W.M. Stacey, Nuclear Reactor Physics, First Edit, Wiley-VCH, 2001.

[10] W.B. Wilson, S.T. Cowell, T.R. England, A.C. Hayes, P. Moller, A Manual for CINDER'90 Version 07.4 Codes and Data, 2008.

[11] A.D. Croff, A User's Manual for the ORIGEN2 Computer Code, 1980.

[12] D. Reilly, N. Ensslin, H. Smith Jr., S. Kreiner, Passive Nondestructive Assay of Nuclear Materials, National Technical Information Service, ISBN 0-16-032724-5, 1991.

[13] P.M. Rinard, G.E. Bosler, Safeguarding LWR Spent Fuel with the Fork Detector, LA-11096-MS, 1988.

[14] A. Lebrun, M. Merelli, J.-L. Szabo, M. Huver, R. Arlt, J. Arenas-Carrasco, SMOPY a New NDA Tool for Safeguards of LEU and MOX Spent Fuel, 2014. http://www-pub.iaea.org/MTCD/publications/PDF/ss-2001/PDF files/Session 14/Paper 14-03.pdf.

[15] R.L. Mössbauer, Kernresonanzfluoreszenz von Gammastrahlung in Ir191, Zeitschrift Für Phys. A. 151 (1958) 124–143.

[16] W. Bertozzi, J. a. Caggiano, W.K. Hensley, M.S. Johnson, S.E. Korbly, R.J. Ledoux, et al., Nuclear resonance fluorescence excitations near 2 MeV in U235 and Pu239, Phys. Rev. C - Nucl. Phys. 78 (2008) 1–5. doi:10.1103/PhysRevC.78.041601.

[17] B.J. Quiter, Nuclear Resonance Fluorescence for Nuclear Materials Assay, Dissertation from University of California Berkeley, (2010).

[18] V. Mozin, S.J. Tobin, L.W. Cambell, J.R. Cheatham, C.R. Freeman, C.J. Gesh, et al., Determining Plutonium Mass in Spent Fuel with Non-destructive Assay Techniques – NGSI Research Overview and Update on NDA Techniques , Part II 2 . Delayed Gamma (DG), IAEA Symp. Int. Safegurads, IAEA-CN-184/137. (2010).

[19] F. Zijderhand, C. Van Der Leun, A New Source of Tuneable Monoenergetic Gamma-Rays, Phys. Lett. 166 (1986) 389–391.

[20] F. Albert, S.G. Anderson, D.J. Gibson, R. a. Marsh, S.S. Wu, C.W. Siders, et al., Design of narrow-band Compton scattering sources for nuclear resonance fluorescence, Phys. Rev. Spec. Top. - Accel. Beams. 14 (2011) 1–11. doi:10.1103/PhysRevSTAB.14.050703.

[21] F. V Hartemann, F. Albert, G.G. Anderson, S.G. Anderson, A.J. Bayramian, S.M. Betts, et al., Overview of mono-energetic gamma-ray sources & applications*, (n.d.) 2129–2131.

[22] C.P.J. Barty, Nuclear photonics with laser-based gamma-rays, IEEE Photonic Soc. 24th Annu. Meet. PHO 2011. 3 (2011) 638–639. doi:10.1109/PHO.2011.6110710.

[23] F. Albert, S.G. Anderson, G. a Anderson, S.M. Betts, D.J. Gibson, C. a Hagmann, et al., Isotope-specific detection of low-density materials with laser-based monoenergetic gamma-rays., Opt. Lett. 35 (2010) 354–356. doi:10.1364/OL.35.000354.

[24] C.P.J. Barty, Extreme Light for Nuclear Photonics, Lawrence Livermore National Laboratory, ELI-Beamlines & HILASE Summer School Presentation, (2014).

[25] S.G. Anderson, F. Albert, a. J. Bayramian, G. Beer, R.E. Bonanno, R.R. Cross, et al., VELOCIRAPTOR: An X-band photoinjector and linear accelerator for the production of Mono-Energetic γ - s, Nucl. Instruments Methods Phys. Res. Sect. A Accel. Spectrometers, Detect. Assoc. Equip. 657 (2011) 140–149. doi:10.1016/j.nima.2011.06.106.

[26] B.A. Ludewigt, B.J. Quiter, S.D. Ambers, Nuclear Resonance Fluorescence for Safeguards Applications, 2011. http://www.osti.gov/bridge/purl.cover.jsp?purl=/1022713-C2tDKO/.

[27] B.A. Ludewigt, B.J. Quiter, S.D. Ambers, Nuclear Resonance Fluorescence to Measure Plutonium Mass in Spent Nuclear Fuel, 2011. http://www.osti.gov/scitech/servlets/purl/1015332/.

[28] T. Shizuma, T. Hayakawa, C.T. Angell, R. Hajima, F. Minato, K. Suyama, et al., Statistical uncertainties of nondestructive assay for spent nuclear fuel by using nuclear resonance fluorescence, Nucl. Instruments Methods Phys. Res. Sect. A Accel. Spectrometers, Detect. Assoc. Equip. 737 (2014) 170–175. doi:10.1016/j.nima.2013.11.069.

[29] M. Omer, H. Negm, H. Ohgaki, I. Daito, T. Hayakawa, M. Bakr, et al., Analysis of nuclear resonance fluorescence excitation measured with LaBr3(Ce) detectors near 2MeV, Nucl. Instruments Methods Phys. Res. Sect. A Accel. Spectrometers, Detect. Assoc. Equip. 729 (2013) 102–107. doi:10.1016/j.nima.2013.06.083.

[30] M.S. Johnson, D.P. Mcnabb, J.M. Hall, Preliminary Study of the Efficacy of Using Nuclear Resonance Fluorescence with Sources for Nuclear Safeguards Assay, LLNL-TR-483851, 2011.

[31] J. Pruet, D. Lange, Contraband Detection with Nuclear Resonance Fluorescence : Feasibility and Impact, UCL-TR-227067, 2007.

[32] L.S. Waters, MCNPX User's manual version 2.3.0, LA-UR-02-2607, (2002) 174.

[33] B.J. Quiter, B. a. Ludewigt, V. V. Mozin, C. Wilson, S. Korbly, Transmission nuclear resonance fluorescence measurements of 238U in thick targets, Nucl. Instruments Methods Phys. Res. Sect. B Beam Interact. with Mater. Atoms. 269 (2011) 1130–1139. doi:10.1016/j.nimb.2011.02.081.

[34] C.P.J. Barty, United States Patent, Patent Number: US8,369,480 B2, Date of Patent: Feb. 5, 2013.

[35] M.L. Fensin, S.J. Tobin, N.P. Sandoval, S.J. Thompson, M.T. Swinhoe, A Monte Carlo Linked Depletion Spent Fuel Library for Assessing Varied Nondestructive Assay Techniques for Nuclear Safeguards, in: Adv. Nucl. Fuel Manag., 2009.

[36] G.F. Knoll, Radiation Detection and Measurement, Third Edit, John Wiley & Sons, Inc, ISBN 978-471-07338-3, 2000.

[37] R.M. Buck, D.P. Heinrichs, C.K. Lee, E.M. Lent, COG11 . 1 Description, New Features, and Development Activities, LLNL-CONF-640038, (2013) 1–7.

APPENDIX A

EXAMPLE COG INPUT OF INTIAL GEOMETRY FROM SECTION 2.2

```
Assembly Test for Pu239 NRF

$    Test for NRF absorption and emission for Pu239 in a spent fuel assembly.
$    Jeremy Gerhart 6/1/14

$    ++++++
$    Source
$    ++++++

$    Energy Distribution: Delta function centered at 2.143570 MeV
$    Spatial Distribution: Point source at X = -2.0 cm
$    Angular Distribution: Fixed angle along + X-axis

$   ++++++++
$    Geometry
$    ++++++++

$    Sample:  One row of pins from a standard PWR 17x17 fuel assembly
$    Witness: Pure Pu239 cylinder at 88, 0, 0 with R = 1.0 cm and H = 0.1 cm
$     Detector: Hemisphere NaI detector array (4"x4"x16" crystals) around the
witness piece, 10 cm standoff
$    Shield: Pure Tungsten plate upstream of the witness detector with X = 15.0
cm Y = 200 cm and Z = 200 cm

$    +++++++
$    Other
$    +++++++

$    NRF reactions enabled
$    First Detector binning is zoomed in for the NRF emission lines

BASIC

    nrf
    photon
    cm
    MeV
    sec

    RN  24468  12125  1 $ Sets random number seeds to obtain the same results
across runs

SURFACES

$   Source

    1      sphere       0.500                          $ Source Void
                TR     -2.000   0.000   0.000

$    Sample
```

```
1025    cylinder     0.475    197.050    -183.050    $ Fuel Pin, Cladding
                TR     0.00      0.00    0.00
                       0.00      0.00    1.00
1026    cylinder     0.420    197.000    -183.000    $ Fuel Pin, Gap
                TR     0.00      0.00    0.00
                       0.00      0.00    1.00
1027    cylinder     0.410    182.760    -183.000    $ Fuel Pin, Fuel
                TR     0.00      0.00    0.00
                       0.00      0.00    1.00

1076    cylinder     0.475    197.050    -183.050    $ Fuel Pin, Cladding
                TR     1.26      0.00    0.00
                       1.26      0.00    1.00
1077    cylinder     0.420    197.000    -183.000    $ Fuel Pin, Gap
                TR     1.26      0.00    0.00
                       1.26      0.00    1.00
1078    cylinder     0.410    182.760    -183.000    $ Fuel Pin, Fuel
                TR     1.26      0.00    0.00
                       1.26      0.00    1.00

1127    cylinder     0.475    197.050    -183.050    $ Fuel Pin, Cladding
                TR     2.52      0.00    0.00
                       2.52      0.00    1.00
1128    cylinder     0.420    197.000    -183.000    $ Fuel Pin, Gap
                TR     2.52      0.00    0.00
                       2.52      0.00    1.00
1129    cylinder     0.410    182.760    -183.000    $ Fuel Pin, Fuel
                TR     2.52      0.00    0.00
                       2.52      0.00    1.00

1178    cylinder     0.475    197.050    -183.050    $ Fuel Pin, Cladding
                TR     3.78      0.00    0.00
                       3.78      0.00    1.00
1179    cylinder     0.420    197.000    -183.000    $ Fuel Pin, Gap
                TR     3.78      0.00    0.00
                       3.78      0.00    1.00
1180    cylinder     0.410    182.760    -183.000    $ Fuel Pin, Fuel
                TR     3.78      0.00    0.00
                       3.78      0.00    1.00

1229    cylinder     0.475    197.050    -183.050    $ Fuel Pin, Cladding
                TR     5.04      0.00    0.00
                       5.04      0.00    1.00
1230    cylinder     0.420    197.000    -183.000    $ Fuel Pin, Gap
                TR     5.04      0.00    0.00
                       5.04      0.00    1.00
1231    cylinder     0.410    182.760    -183.000    $ Fuel Pin, Fuel
                TR     5.04      0.00    0.00
                       5.04      0.00    1.00

1280    cylinder     0.475    197.050    -183.050    $ Fuel Pin, Cladding
                TR     6.30      0.00    0.00
                       6.30      0.00    1.00
1281    cylinder     0.420    197.000    -183.000    $ Fuel Pin, Gap
                TR     6.30      0.00    0.00
                       6.30      0.00    1.00
1282    cylinder     0.410    182.760    -183.000    $ Fuel Pin, Fuel
                TR     6.30      0.00    0.00
                       6.30      0.00    1.00
```

```
1331    cylinder     0.475    197.050    -183.050    $ Fuel Pin, Cladding
                TR     7.56      0.00    0.00
                       7.56      0.00    1.00
1332    cylinder     0.420    197.000    -183.000    $ Fuel Pin, Gap
                TR     7.56      0.00    0.00
                       7.56      0.00    1.00
1333    cylinder     0.410    182.760    -183.000    $ Fuel Pin, Fuel
                TR     7.56      0.00    0.00
                       7.56      0.00    1.00

1382    cylinder     0.475    197.050    -183.050    $ Fuel Pin, Cladding
                TR     8.82      0.00    0.00
                       8.82      0.00    1.00
1383    cylinder     0.420    197.000    -183.000    $ Fuel Pin, Gap
                TR     8.82      0.00    0.00
                       8.82      0.00    1.00
1384    cylinder     0.410    182.760    -183.000    $ Fuel Pin, Fuel
                TR     8.82      0.00    0.00
                       8.82      0.00    1.00

1433    cylinder     0.475    197.050    -183.050    $ Fuel Pin, Cladding
                TR    10.08      0.00    0.00
                      10.08      0.00    1.00
1434    cylinder     0.420    197.000    -183.000    $ Fuel Pin, Gap
                TR    10.08      0.00    0.00
                      10.08      0.00    1.00
1435    cylinder     0.410    182.760    -183.000    $ Fuel Pin, Fuel
                TR    10.08      0.00    0.00
                      10.08      0.00    1.00

1484    cylinder     0.475    197.050    -183.050    $ Fuel Pin, Cladding
                TR    11.34      0.00    0.00
                      11.34      0.00    1.00
1485    cylinder     0.420    197.000    -183.000    $ Fuel Pin, Gap
                TR    11.34      0.00    0.00
                      11.34      0.00    1.00
1486    cylinder     0.410    182.760    -183.000    $ Fuel Pin, Fuel
                TR    11.34      0.00    0.00
                      11.34      0.00    1.00

1535    cylinder     0.475    197.050    -183.050    $ Fuel Pin, Cladding
                TR    12.60      0.00    0.00
                      12.60      0.00    1.00
1536    cylinder     0.420    197.000    -183.000    $ Fuel Pin, Gap
                TR    12.60      0.00    0.00
                      12.60      0.00    1.00
1537    cylinder     0.410    182.760    -183.000    $ Fuel Pin, Fuel
                TR    12.60      0.00    0.00
                      12.60      0.00    1.00

1586    cylinder     0.475    197.050    -183.050    $ Fuel Pin, Cladding
                TR    13.86      0.00    0.00
                      13.86      0.00    1.00
1587    cylinder     0.420    197.000    -183.000    $ Fuel Pin, Gap
                TR    13.86      0.00    0.00
                      13.86      0.00    1.00
1588    cylinder     0.410    182.760    -183.000    $ Fuel Pin, Fuel
                TR    13.86      0.00    0.00
```

```
                          13.86     0.00   1.00

    1637    cylinder     0.475    197.050    -183.050    $ Fuel Pin, Cladding
                    TR    15.12     0.00   0.00
                          15.12     0.00   1.00
    1638    cylinder     0.420    197.000    -183.000    $ Fuel Pin, Gap
                    TR    15.12     0.00   0.00
                          15.12     0.00   1.00
    1639    cylinder     0.410    182.760    -183.000    $ Fuel Pin, Fuel
                    TR    15.12     0.00   0.00
                          15.12     0.00   1.00

    1688    cylinder     0.475    197.050    -183.050    $ Fuel Pin, Cladding
                    TR    16.38     0.00   0.00
                          16.38     0.00   1.00
    1689    cylinder     0.420    197.000    -183.000    $ Fuel Pin, Gap
                    TR    16.38     0.00   0.00
                          16.38     0.00   1.00
    1690    cylinder     0.410    182.760    -183.000    $ Fuel Pin, Fuel
                    TR    16.38     0.00   0.00
                          16.38     0.00   1.00

    1739    cylinder     0.475    197.050    -183.050    $ Fuel Pin, Cladding
                    TR    17.64     0.00   0.00
                          17.64     0.00   1.00
    1740    cylinder     0.420    197.000    -183.000    $ Fuel Pin, Gap
                    TR    17.64     0.00   0.00
                          17.64     0.00   1.00
    1741    cylinder     0.410    182.760    -183.000    $ Fuel Pin, Fuel
                    TR    17.64     0.00   0.00
                          17.64     0.00   1.00

    1790    cylinder     0.475    197.050    -183.050    $ Fuel Pin, Cladding
                    TR    18.90     0.00   0.00
                          18.90     0.00   1.00
    1791    cylinder     0.420    197.000    -183.000    $ Fuel Pin, Gap
                    TR    18.90     0.00   0.00
                          18.90     0.00   1.00
    1792    cylinder     0.410    182.760    -183.000    $ Fuel Pin, Fuel
                    TR    18.90     0.00   0.00
                          18.90     0.00   1.00

    1841    cylinder     0.475    197.050    -183.050    $ Fuel Pin, Cladding
                    TR    20.16     0.00   0.00
                          20.16     0.00   1.00
    1842    cylinder     0.420    197.000    -183.000    $ Fuel Pin, Gap
                    TR    20.16     0.00   0.00
                          20.16     0.00   1.00
    1843    cylinder     0.410    182.760    -183.000    $ Fuel Pin, Fuel
                    TR    20.16     0.00   0.00
                          20.16     0.00   1.00

$    Witness Shield

    301    box        15.000    200.000     200.000    $ Shield Boundary
                TR    30.000      0.000       0.000
    302    cylinder    0.250                            $ Beam Aperture

$    Witness Detector
```

```
    401    box        10.130     10.160      40.640         $  positive  y-axis
alignment
                  TR    88.000     30.820       0.000
                        89.000     30.820       0.000
                        88.000     30.820       1.000

    402    box        10.130     10.160      40.640         $  negative  y-axis
alignment
                  TR    88.000    -30.820       0.000
                        89.000    -30.820       0.000
                       88.000    -30.820       1.000

       403    box        10.130     10.160      40.640      $  positive  z-axis
alignment
                  TR    88.000      0.000      30.820
                        89.000      0.000      30.820
                        88.000      1.000      30.820

       404    box        10.130     10.160      40.640      $  negative  z-axis
alignment
                  TR    88.000      0.000     -30.820
                        89.000      0.000     -30.820
                        88.000      1.000     -30.820

       405    box        10.130     10.160      40.640      $ positive 135 xz-
axis alignment
                  TR    64.957      0.000      21.293
                        65.957      0.000      22.293
                        64.957      1.000      21.293

       406    box        10.130     10.160      40.640      $ negative 135 xz-
axis alignment
                  TR    64.957      0.000     -21.293
                      63.957      0.000     -20.293
                             64.957      1.000     -21.293

       407    box        10.130     10.160      40.640      $ positive 135 xy-
axis alignment
                  TR    64.957     21.293       0.000
                        65.957     22.293       0.000
                        64.957     21.293       1.000

       408    box        10.130     10.160      40.640      $ negative 135 xy-
axis alignment
                  TR    64.957    -21.293       0.000
                        63.957    -20.293       0.000
                        64.957    -21.293       1.000

$    Witness Piece

    501    cylinder     1.000      0.050      -0.050    $ Witness Boundary
                  TR    88.000      0.000       0.000
                           89.000      0.000       0.000

$    Boundary

    999    box        500.000    500.000     500.000    $ Boundary
```

```
GEOMETRY

$   Source

    sector      1    srcsph      -1                    $ Source Void

$    Sample

    sector    1025    pincld    -1025    1026             $ Fuel Pin, Cladding
    sector    1026    pingap    -1026    1027             $ Fuel Pin, Gap
    sector    1027    pinful    -1027                     $ Fuel Pin, Fuel

    sector    1076    pincld    -1076    1077             $ Fuel Pin, Cladding
    sector    1077    pingap    -1077    1078             $ Fuel Pin, Gap
    sector    1078    pinful    -1078                     $ Fuel Pin, Fuel

    sector    1127    pincld    -1127    1128             $ Fuel Pin, Cladding
    sector    1128    pingap    -1128    1129             $ Fuel Pin, Gap
    sector    1129    pinful    -1129                     $ Fuel Pin, Fuel

    sector    1178    pincld    -1178    1179             $ Fuel Pin, Cladding
    sector    1179    pingap    -1179    1180             $ Fuel Pin, Gap
    sector    1180    pinful    -1180                     $ Fuel Pin, Fuel

    sector    1229    pincld    -1229    1230             $ Fuel Pin, Cladding
    sector    1230    pingap    -1230    1231             $ Fuel Pin, Gap
    sector    1231    pinful    -1231                     $ Fuel Pin, Fuel

    sector    1280    pincld    -1280    1281             $ Fuel Pin, Cladding
    sector    1281    pingap    -1281    1282             $ Fuel Pin, Gap
    sector    1282    pinful    -1282                     $ Fuel Pin, Fuel

    sector    1331    pincld    -1331    1332             $ Fuel Pin, Cladding
    sector    1332    pingap    -1332    1333             $ Fuel Pin, Gap
    sector    1333    pinful    -1333                     $ Fuel Pin, Fuel

    sector    1382    pincld    -1382    1383             $ Fuel Pin, Cladding
    sector    1383    pingap    -1383    1384             $ Fuel Pin, Gap
    sector    1384    pinful    -1384                     $ Fuel Pin, Fuel

    sector    1433    pincld    -1433    1434             $ Fuel Pin, Cladding
    sector    1434    pingap    -1434    1435             $ Fuel Pin, Gap
    sector    1435    pinful    -1435                     $ Fuel Pin, Fuel

    sector    1484    pincld    -1484    1485             $ Fuel Pin, Cladding
    sector    1485    pingap    -1485    1486             $ Fuel Pin, Gap
    sector    1486    pinful    -1486                     $ Fuel Pin, Fuel

    sector    1535    pincld    -1535    1536             $ Fuel Pin, Cladding
    sector    1536    pingap    -1536    1537             $ Fuel Pin, Gap
    sector    1537    pinful    -1537                     $ Fuel Pin, Fuel

    sector    1586    pincld    -1586    1587             $ Fuel Pin, Cladding
    sector    1587    pingap    -1587    1588             $ Fuel Pin, Gap
    sector    1588    pinful    -1588                     $ Fuel Pin, Fuel

    sector    1637    pincld    -1637    1638             $ Fuel Pin, Cladding
    sector    1638    pingap    -1638    1639             $ Fuel Pin, Gap
    sector    1639    pinful    -1639                     $ Fuel Pin, Fuel
```

```
    sector    1688    pincld    -1688    1689             $ Fuel Pin, Cladding
    sector    1689    pingap    -1689    1690             $ Fuel Pin, Gap
    sector    1690    pinful    -1690                     $ Fuel Pin, Fuel

    sector    1739    pincld    -1739    1740             $ Fuel Pin, Cladding
    sector    1740    pingap    -1740    1741             $ Fuel Pin, Gap
    sector    1741    pinful    -1741                     $ Fuel Pin, Fuel

    sector    1790    pincld    -1790    1791             $ Fuel Pin, Cladding
    sector    1791    pingap    -1791    1792             $ Fuel Pin, Gap
    sector    1792    pinful    -1792                     $ Fuel Pin, Fuel

    sector    1841    pincld    -1841    1842             $ Fuel Pin, Cladding
    sector    1842    pingap    -1842    1843             $ Fuel Pin, Gap
    sector    1843    pinful    -1843                     $ Fuel Pin, Fuel

$    Witness Shield

    sector    301    wtshld    -301    302              $ Witness Shield

$   Witness Detector

    sector    401    detin1    -401
    sector    402    detin2    -402
    sector    403    detin3    -403
    sector    404    detin4    -404
    sector    405    detin5    -405
    sector    406    detin6    -406
    sector    407    detin7    -407
    sector    408    detin8    -408

$   Witness Piece

    sector    501    witpce    -501                     $ Witness Piece

$    Boundary

    fill                         999                   $ Fill Volume
    boundary         vacuum      999                   $ Vacuum Boundary

MIX

    mat   =   1  A-F  1.0  Zr90      0.511754     $ Zircaloy Fuel Cladding
                                       Zr94      0.172871
                                       Zr92      0.170581
                                    Zr91      0.111601
                                    Zr96      0.027851
                                    Fe56      0.003151
                                    Cr52      0.001472
                                           Fe54      0.000201
                                           Cr53      0.000167
                                     H1        0.000150
                                     Cr50      0.000076
                                     Fe57      0.000073
                                     Cr54      0.000042
                                     Fe58      0.000010

    mat   =   2  A-F  1.0  He4       1.000000     $ Fuel Gap
```

```
    mat    =    3  A-F  1.0  O16       0.677773     $ Freshly Burned Fuel Pin 4%
45GWD
                                    U238     0.314785
                                  U235     0.002332
                                  U236     0.001895
                                  Pu239    0.001505
                                  Pu240    0.000930
                                  Pu241    0.000434
                                  Pu242    0.000274
                                  Pu238    0.000274

    mat    =    4  A-F  1.0  N         9.7624E-04   $ Air at STP
                                    O         3.0010E-04
                                    Ar        1.6557E-04

    mat    =    5  A-F  1.0  W        1.000000     $ Tungsten

    mat    =    6  A-F  1.0  Pu239    1.000000     $ Plutonium

       mat    =    7  A-F  1.0  Na        0.500000     $ NaI Detector
                                        I         0.500000

ASSIGN-MD

$   Source

      1     0      1.000000     $ Source Void

$    Sample

    1025     1      6.440000     $ Fuel Pin, Cladding
    1026     2      0.000781     $ Fuel Pin, Gap
    1027     3     10.438730     $ Fuel Pin, Fuel

    1076     1      6.440000     $ Fuel Pin, Cladding
    1077     2      0.000781     $ Fuel Pin, Gap
    1078     3     10.438730     $ Fuel Pin, Fuel

    1127     1      6.440000     $ Fuel Pin, Cladding
    1128     2      0.000781     $ Fuel Pin, Gap
    1129     3     10.438730     $ Fuel Pin, Fuel

    1178     1      6.440000     $ Fuel Pin, Cladding
    1179     2      0.000781     $ Fuel Pin, Gap
    1180     3     10.438730     $ Fuel Pin, Fuel

    1229     1      6.440000     $ Fuel Pin, Cladding
    1230     2      0.000781     $ Fuel Pin, Gap
    1231     3     10.438730     $ Fuel Pin, Fuel

    1280     1      6.440000     $ Fuel Pin, Cladding
    1281     2      0.000781     $ Fuel Pin, Gap
    1282     3     10.438730     $ Fuel Pin, Fuel

    1331     1      6.440000     $ Fuel Pin, Cladding
    1332     2      0.000781     $ Fuel Pin, Gap
    1333     3     10.438730     $ Fuel Pin, Fuel
```

```
    1382     1      6.440000     $ Fuel Pin, Cladding
    1383     2      0.000781     $ Fuel Pin, Gap
    1384     3     10.438730     $ Fuel Pin, Fuel

    1433     1      6.440000     $ Fuel Pin, Cladding
    1434     2      0.000781     $ Fuel Pin, Gap
    1435     3     10.438730     $ Fuel Pin, Fuel

    1484     1      6.440000     $ Fuel Pin, Cladding
    1485     2      0.000781     $ Fuel Pin, Gap
    1486     3     10.438730     $ Fuel Pin, Fuel

    1535     1      6.440000     $ Fuel Pin, Cladding
    1536     2      0.000781     $ Fuel Pin, Gap
    1537     3     10.438730     $ Fuel Pin, Fuel

    1586     1      6.440000     $ Fuel Pin, Cladding
    1587     2      0.000781     $ Fuel Pin, Gap
    1588     3     10.438730     $ Fuel Pin, Fuel

    1637     1      6.440000     $ Fuel Pin, Cladding
    1638     2      0.000781     $ Fuel Pin, Gap
    1639     3     10.438730     $ Fuel Pin, Fuel

    1688     1      6.440000     $ Fuel Pin, Cladding
    1689     2      0.000781     $ Fuel Pin, Gap
    1690     3     10.438730     $ Fuel Pin, Fuel

    1739     1      6.440000     $ Fuel Pin, Cladding
    1740     2      0.000781     $ Fuel Pin, Gap
    1741     3     10.438730     $ Fuel Pin, Fuel

    1790     1      6.440000     $ Fuel Pin, Cladding
    1791     2      0.000781     $ Fuel Pin, Gap
    1792     3     10.438730     $ Fuel Pin, Fuel

    1841     1      6.440000     $ Fuel Pin, Cladding
    1842     2      0.000781     $ Fuel Pin, Gap
    1843     3     10.438730     $ Fuel Pin, Fuel

$    Witness Shield

    301     -1     19.250000     $ Witness Shield

$    Witness Detector

    401     7      3.670000
    402     7      3.670000
    403     7      3.670000
    404     7      3.670000
      405     7      3.670000
      406     7      3.670000
      407     7      3.670000
      408     7      3.670000

$    Witness Piece

    501     6     19.816000     $ Witness Piece
```

```
$    Boundary

    999     0      1.000000     $ Vacuum

ASSIGN-RL

       400  401  402  403  404  405  406  407  408  $NaI Detector Array

SOURCE

       nparticles       =  1000000000

       define position  =  1
                           point     -2.0000      0.0000      0.0000

       define position  =  2
                           ss-disk   -2 0 0  -1 0 0  0.005642  0

       define energy    =  1
                           photon
                      distribution   2.143567E+00   1.000000E+00
                                                    2.143573E+00   1.000000E+00

       define energy    =  2
                           photon
                      gaussian       2.143570E+00   5.887500E-3

       define time      =  1
                           steady

       define angle     =  1
                           1.0000    0.0000    0.0000
                      fixed

       increment  1.000000E+00  position    =  1              $ Point Source
                                                  energy     =  1            $
Pu239 NRF
$                                 time        =  1              $ Steady State
                                  angle       =  1              $ Fixed Beam
                                  importance  =  1.000000E+00

DETECTOR

       number   =  naiarr1
         title  =  "Pu239 NRF Spectrum from NaI Array (reaction type)"
         pulse  [400,0]  $ 8 4x4x16 NaI Crystals
         bin  energy  photon  $  2 eV wide bins bracket emission lines
          0.000000E+00  7.850000E-03  7.852000E-03  7.854000E-03
          7.856000E-03  7.858000E-03  7.860000E-03  7.862000E-03
          7.864000E-03  7.866000E-03  7.868000E-03  7.870000E-03
          7.872000E-03  1.000000E-02  2.000000E-02  3.000000E-02
          4.000000E-02  5.000000E-02  6.000000E-02  7.000000E-02
          8.000000E-02  9.000000E-02  1.000000E-01  1.100000E-01
          1.200000E-01  1.300000E-01  1.400000E-01  1.500000E-01
          1.600000E-01  1.700000E-01  1.800000E-01  1.900000E-01
          2.000000E-01  2.100000E-01  2.200000E-01  2.300000E-01
          2.400000E-01  2.500000E-01  2.600000E-01  2.700000E-01
          2.800000E-01  2.900000E-01  3.000000E-01  3.100000E-01
          3.200000E-01  3.300000E-01  3.400000E-01  3.500000E-01
```

3.600000E-01 3.700000E-01 3.800000E-01 3.900000E-01
4.000000E-01 4.100000E-01 4.200000E-01 4.300000E-01
4.400000E-01 4.500000E-01 4.600000E-01 4.700000E-01
4.800000E-01 4.900000E-01 5.000000E-01 5.100000E-01
5.200000E-01 5.300000E-01 5.400000E-01 5.500000E-01
5.600000E-01 5.700000E-01 5.800000E-01 5.900000E-01
6.000000E-01 6.100000E-01 6.200000E-01 6.300000E-01
6.400000E-01 6.500000E-01 6.600000E-01 6.700000E-01
6.800000E-01 6.900000E-01 7.000000E-01 7.100000E-01
7.200000E-01 7.300000E-01 7.400000E-01 7.500000E-01
7.600000E-01 7.700000E-01 7.800000E-01 7.900000E-01
8.000000E-01 8.100000E-01 8.200000E-01 8.300000E-01
8.400000E-01 8.500000E-01 8.600000E-01 8.700000E-01
8.800000E-01 8.900000E-01 9.000000E-01 9.100000E-01
9.200000E-01 9.300000E-01 9.400000E-01 9.500000E-01
9.600000E-01 9.700000E-01 9.800000E-01 9.900000E-01
1.000000E+00 1.010000E+00 1.020000E+00 1.030000E+00
1.040000E+00 1.050000E+00 1.060000E+00 1.070000E+00
1.080000E+00 1.090000E+00 1.100000E+00 1.110000E+00
1.120000E+00 1.130000E+00 1.140000E+00 1.150000E+00
1.160000E+00 1.170000E+00 1.180000E+00 1.190000E+00
1.200000E+00 1.210000E+00 1.220000E+00 1.230000E+00
1.240000E+00 1.250000E+00 1.260000E+00 1.270000E+00
1.280000E+00 1.290000E+00 1.300000E+00 1.310000E+00
1.320000E+00 1.330000E+00 1.340000E+00 1.350000E+00
1.360000E+00 1.370000E+00 1.380000E+00 1.390000E+00
1.400000E+00 1.410000E+00 1.420000E+00 1.430000E+00
1.440000E+00 1.450000E+00 1.460000E+00 1.470000E+00
1.480000E+00 1.490000E+00 1.500000E+00 1.510000E+00
1.520000E+00 1.530000E+00 1.540000E+00 1.550000E+00
1.560000E+00 1.570000E+00 1.580000E+00 1.590000E+00
1.600000E+00 1.610000E+00 1.620000E+00 1.630000E+00
1.640000E+00 1.650000E+00 1.660000E+00 1.670000E+00
1.680000E+00 1.690000E+00 1.700000E+00 1.710000E+00
1.720000E+00 1.730000E+00 1.740000E+00 1.750000E+00
1.760000E+00 1.770000E+00 1.780000E+00 1.790000E+00
1.800000E+00 1.810000E+00 1.820000E+00 1.830000E+00
1.840000E+00 1.850000E+00 1.860000E+00 1.870000E+00
1.880000E+00 1.890000E+00 1.900000E+00 1.910000E+00
1.920000E+00 1.930000E+00 1.940000E+00 1.950000E+00
1.960000E+00 1.970000E+00 1.980000E+00 1.990000E+00
2.000000E+00 2.010000E+00 2.020000E+00 2.030000E+00
2.040000E+00 2.050000E+00 2.060000E+00 2.070000E+00
2.080000E+00 2.090000E+00 2.100000E+00 2.110000E+00
2.120000E+00 2.130000E+00 2.135678E+00 2.135680E+00
2.135682E+00 2.135684E+00 2.135686E+00 2.135688E+00
2.135690E+00 2.135692E+00 2.135694E+00 2.135696E+00
2.135698E+00 2.135700E+00 2.140000E+00 2.143539E+00
2.143541E+00 2.143543E+00 2.143545E+00 2.143547E+00
2.143549E+00 2.143551E+00 2.143553E+00 2.143555E+00
2.143557E+00 2.143559E+00 2.143561E+00 2.150000E+00
2.160000E+00 2.170000E+00 2.180000E+00 2.190000E+00
2.200000E+00 2.210000E+00 2.220000E+00 2.230000E+00
2.240000E+00 2.250000E+00 2.260000E+00 2.270000E+00
2.280000E+00 2.290000E+00 2.300000E+00 2.310000E+00
2.320000E+00 2.330000E+00 2.340000E+00 2.350000E+00
2.360000E+00 2.370000E+00 2.380000E+00 2.390000E+00
2.400000E+00 2.410000E+00 2.420000E+00 2.430000E+00
2.440000E+00 2.450000E+00 2.460000E+00 2.470000E+00

```
  2.480000E+00  2.490000E+00  2.500000E+00
Elabel  =  "Photon Energy [MeV]"
Ylabel  =  "Differential Response [Flux/Mev/s]"

END
```

APPENDIX B

EXAMPLE OF COG INPUT FOR SIMPLE GEOMETRY IN SECTION 3

```
Block Test for Pu239 NRF

$    Test for NRF absorption and emission for Pu239 in a 239Pu and 238U cube.
$    Jeremy Gerhart 6/1/14

$    ++++++
$    Source
$    ++++++

$    Energy Distribution: Delta function centered at 2.143570 MeV

$   ++++++++
$    Geometry
$    ++++++++

$    Sample:  A 1 cm by 1 cm by 1 cm cube.
$    Detector: Cylindrical surface detector positioned down stream of block

$    +++++++
$    Other
$    +++++++

$    NRF reactions enabled
$    First Detector binning is zoomed in for the NRF emission lines

BASIC

    nrf
    photon
    cm
    MeV
    sec

    RN  24468  12125  1 $ Sets random number seeds to obtain the same results
across runs

SURFACES

$   Source

    1      sphere       0.500                          $ Source Void

$    Sample

    101    box      1.000  1.000  1.000
                   TR  1.000  0.000  0.000

$    Detector

    201    cylinder     0.500      0.000       0.500    $ Detector Boundary
                TR    19.000      0.000       0.000
```

```
                          20.000      0.000       0.000

    202    cylinder     0.500      0.000       0.500    $ Detector Boundary
                 TR    19.500      0.000       0.000
                          20.500      0.000       0.000

$    Boundary

    999    box        100.000    100.000     100.000    $ Boundary

GEOMETRY

$   Source

    sector      1    srcsph      -1                     $ Source Void

$    Sample

    sector    101    pusam1      -101

$   Detector

    sector    201    detin1    -201
    sector    202    detin2    -202

$    Boundary

    fill                         999                    $ Fill Volume
    boundary         vacuum      999                    $ Vacuum Boundary

MIX

    mat   =   1  A-F  1.0  U238   0.99
                              Pu239    0.01

ASSIGN-MD

$   Source

      1     0      1.000000     $ Source Void

$    Sample

    101     1     10.438730

$    Witness Detector

    201     0      1.000000
    202     0      1.000000

$    Boundary

    999     0      1.000000     $ Vacuum

SOURCE

       nparticles       =  1000000

       define position  =  1
```

```
                        point     -2.0000      0.0000      0.0000

      define position  =  2
                         ss-disk   -2 0 0  -1 0 0  0.005642  0

      define energy    =  1
                         photon
                    distribution   2.143567E+00   1.000000E+00
                                   2.143573E+00   1.000000E+00

      define energy    =  2
                         photon
                    gaussian       2.143570E+00   5.887500E-3

      define time      =  1
                         steady

      define angle     =  1
                         1.0000    0.0000    0.0000
                    fixed

      increment  1.000000E+00  position    =  1              $ Point Source
                                                 energy     =  1            $
Pu239 NRF
$                                 time        =  1              $ Steady State
                                  angle       =  1              $ Fixed Beam
                                  importance  =  1.000000E+00

DETECTOR

    number   =  dsd01
      title  =  "Down stream detector (counts & espec)"
      boundary  counts  201  202  6.283185E+04
      bin  energy  photon  $  2 eV wide bins bracket emission lines
          0.000000E+00  1.000000E-02  2.000000E-02  3.000000E-02
          4.000000E-02  5.000000E-02  6.000000E-02  7.000000E-02
          8.000000E-02  9.000000E-02  1.000000E-01  1.100000E-01
          1.200000E-01  1.300000E-01  1.400000E-01  1.500000E-01
          1.600000E-01  1.700000E-01  1.800000E-01  1.900000E-01
          2.000000E-01  2.100000E-01  2.200000E-01  2.300000E-01
          2.400000E-01  2.500000E-01  2.600000E-01  2.700000E-01
          2.800000E-01  2.900000E-01  3.000000E-01  3.100000E-01
          3.200000E-01  3.300000E-01  3.400000E-01  3.500000E-01
          3.600000E-01  3.700000E-01  3.800000E-01  3.900000E-01
          4.000000E-01  4.100000E-01  4.200000E-01  4.300000E-01
          4.400000E-01  4.500000E-01  4.600000E-01  4.700000E-01
          4.775840E-01  4.775860E-01  4.775880E-01  4.775900E-01
          4.775920E-01  4.775940E-01  4.775960E-01  4.775980E-01
          4.776000E-01  4.776020E-01  4.776040E-01  4.776060E-01
          4.800000E-01  4.900000E-01  5.000000E-01  5.100000E-01
          5.200000E-01  5.300000E-01  5.400000E-01  5.500000E-01
          5.600000E-01  5.700000E-01  5.800000E-01  5.900000E-01
          6.000000E-01  6.100000E-01  6.200000E-01  6.300000E-01
          6.400000E-01  6.500000E-01  6.600000E-01  6.700000E-01
          6.800000E-01  6.900000E-01  7.000000E-01  7.100000E-01
          7.200000E-01  7.300000E-01  7.400000E-01  7.500000E-01
          7.600000E-01  7.700000E-01  7.800000E-01  7.900000E-01
          8.000000E-01  8.100000E-01  8.200000E-01  8.300000E-01
          8.400000E-01  8.500000E-01  8.600000E-01  8.700000E-01
```

```
  8.800000E-01  8.900000E-01  9.000000E-01  9.100000E-01
  9.200000E-01  9.300000E-01  9.400000E-01  9.500000E-01
  9.600000E-01  9.700000E-01  9.800000E-01  9.900000E-01
  1.000000E+00  1.010000E+00  1.020000E+00  1.030000E+00
  1.040000E+00  1.050000E+00  1.060000E+00  1.070000E+00
  1.080000E+00  1.090000E+00  1.100000E+00  1.110000E+00
  1.120000E+00  1.130000E+00  1.140000E+00  1.150000E+00
  1.160000E+00  1.170000E+00  1.180000E+00  1.190000E+00
  1.200000E+00  1.210000E+00  1.220000E+00  1.230000E+00
  1.240000E+00  1.250000E+00  1.260000E+00  1.270000E+00
  1.280000E+00  1.290000E+00  1.300000E+00  1.310000E+00
  1.320000E+00  1.330000E+00  1.340000E+00  1.350000E+00
  1.360000E+00  1.370000E+00  1.380000E+00  1.390000E+00
  1.400000E+00  1.410000E+00  1.420000E+00  1.430000E+00
  1.440000E+00  1.450000E+00  1.460000E+00  1.470000E+00
  1.480000E+00  1.490000E+00  1.500000E+00  1.510000E+00
  1.520000E+00  1.530000E+00  1.540000E+00  1.550000E+00
  1.560000E+00  1.570000E+00  1.580000E+00  1.590000E+00
  1.600000E+00  1.610000E+00  1.620000E+00  1.630000E+00
  1.640000E+00  1.650000E+00  1.660000E+00  1.670000E+00
  1.680000E+00  1.690000E+00  1.700000E+00  1.710000E+00
  1.720000E+00  1.730000E+00  1.740000E+00  1.750000E+00
  1.760000E+00  1.770000E+00  1.780000E+00  1.790000E+00
  1.800000E+00  1.810000E+00  1.820000E+00  1.830000E+00
  1.840000E+00  1.850000E+00  1.860000E+00  1.870000E+00
  1.880000E+00  1.890000E+00  1.900000E+00  1.910000E+00
  1.920000E+00  1.930000E+00  1.940000E+00  1.950000E+00
  1.960000E+00  1.970000E+00  1.980000E+00  1.990000E+00
  2.000000E+00  2.010000E+00  2.020000E+00  2.030000E+00
  2.040000E+00  2.050000E+00  2.060000E+00  2.070000E+00
  2.080000E+00  2.090000E+00  2.100000E+00  2.110000E+00
  2.120000E+00  2.130000E+00  2.140000E+00  2.150000E+00
  2.160000E+00  2.170000E+00  2.180000E+00  2.190000E+00
  2.200000E+00  2.210000E+00  2.220000E+00  2.230000E+00
  2.240000E+00  2.250000E+00  2.260000E+00  2.270000E+00
  2.280000E+00  2.290000E+00  2.300000E+00  2.310000E+00
  2.320000E+00  2.330000E+00  2.340000E+00  2.350000E+00
  2.360000E+00  2.370000E+00  2.380000E+00  2.390000E+00
  2.400000E+00  2.410000E+00  2.420000E+00  2.430000E+00
  2.440000E+00  2.450000E+00  2.460000E+00  2.470000E+00
  2.480000E+00  2.490000E+00  2.500000E+00
Elabel  =  "Photon Energy [MeV]"
Ylabel  =  "Differential Response [counts/Mev]"

END
```